Title

Arp2/3 complex activity is necessary for mouse embryonic stem cell differentiation, times formative pluripotency, and enables lineage specification

Author

Aloisio, Francesca Mari

Publication Date

2021

Arp2/3 complex activity is necessary for mouse embryonic stem cell differentiation, times formative pluripotency, and enables lineage specification

by
Francesca Mari Aloisio

DISSERTATION
Submitted in partial satisfaction of the requirements for degree of
DOCTOR OF PHILOSOPHY

in

Biomedical Sciences

in the

GRADUATE DIVISION
of the
UNIVERSITY OF CALIFORNIA, SAN FRANCISCO

Approved:

Julie Beth Sneddon — Julie Beth Sneddon
Chair

Diane Barber — Diane Barber

Todd Nystul — Todd Nystul

Matthew Welch — Matthew Welch

Committee Members

To my grandmothers, Frances Amadeo Aloisio and Eduviges Perla Bielma, and grandfathers, Rosario Aloisio and Eliceo Ruben Bielma, whose courage, strength, and resilience continue to inspire me today and every day.

To my parents, Frank Aloisio and Jacqueline Bielma Aloisio, whose infinite love and support make anything seem possible.

Acknowledgements

Completing this PhD has been the most challenging and rewarding thing I have ever done. There have been many times when I thought I did not have the ability to finish such a colossal undertaking, but I've been very fortunate to have the world's best support system that always pulled me through. To every single person who believed in me, helped me, hugged me, inspired me, or simply made me laugh... thank you so very much.

I am forever grateful to my brilliant, kind, and supportive mentor, Dr. Diane Barber. From the very first time I heard Diane speak about her research, her career, and her family at a pizza talk in Fall 2014, I knew that I wanted to learn everything I possibly could from her. Almost seven years later, I could not be more thrilled with that decision. I am continually in awe at her ability to synthesize her extensive knowledge to ask important questions and pass on her expertise to her trainees, caring for them both inside and outside of the lab. Diane has cultivated my development as a better investigator, communicator, and human being during my time as her inaugural PhD student, carrying me during the lows and flying alongside me during the highs. Above all, Diane has taught me how to find my voice – to be an advocate for myself and for others, a skill that has allowed me to carve a place for myself and for others in academia and beyond. During the last seven years, I have grown in ways I never imagined that I could, and I owe it all to my mentor-extraordinaire, Dr. Diane Barber.

I am also so very grateful to my wider mentor family who have each played a role in my development. Firstly, to my thesis committee, Dr. Julie Sneddon, Dr. Todd Nystul, and Dr. Matthew Welch, whose caring guidance has culminated in the kind of thesis that I am truly proud to put out into the world. Additionally, I am so thankful to all of the wonderful mentors who believed in me and took the time to help me grow as a budding researcher during my undergraduate years. I never could have made it to UCSF without your thoughtful care and support: Dr. Grace Choy, Dr. Sarah Simmons, Dr. Leah Sabin, Dr. Greg Hannon, Dr. James Burke, Dr. Christopher Sullivan, Dr. Ruth Buskirk, Dr. Arturo DeLozanne, and Dr. Therese O'Halloran.

I next must acknowledge the exceptional support from my lab family, The Barber Shop. To members of the Barber Lab, both past and present, I am eternally appreciative that I had the privilege of crossing paths with some of the most extraordinary researchers I've ever met during the very formative years of my graduate training. Each of you has in your own way influenced me to be a more courageous speaker, a more tenacious investigator, and a more creative thinker: Dr. Bree Grillo-Hill, Dr. Katharine White, Dr. Bradley Webb, Dr. Manish Rana, Dr. Yi Liu, Dr. Christos Kougentakis, Kyle Kisor, Nathaniel Meyer, Cambria Chou-Freed, Joy Gittins, Tiffany Criger, Dr. Jeffrey Van Haren, Dr. Rabab Charafeddine, Dr. Alessandro Dema, and Dr. Torsten Wittmann,

Beyond our lab, I am so grateful to the broader research community that has contributed to me being able to make this work a reality. Firstly, UCSF has been such an amazingly supportive and fun place to be a graduate student. A special thanks to:

Demian Sainz, Dr. D'Anne Duncan, Ned Molyneaux, Evolve Benton, Lisa Magargal, Dr. Elizabeth Silva, Dr. Mark Ansel, Dr. Anita Sil, the UCSF Graduate Division, Biomedical Sciences Graduate Program, Department of Cell & Tissue Biology, and HSW6 community both past and present. Additionally, I am thankful to the HHMI Gilliam Fellowship and the UCSF Discovery Fellowship for their generous financial support of this work.

To every longtime friend and supporter who has been a treasured part of my life outside of the lab, thank you from the bottom of my heart: Joana Guthrie, Kathleen Shaffer, Dr. Eric Yoon, Caroline Sprague, Rachel Tessmer, Alla Klussmann, Alexander Brown, Jordan Koenig, Paul Lee, The Taylor AP Squad, Jorge-Felipe Ortíz Carpena, Marimar Benitez de la Vega, Dr. Alexandra Clemente Perez, Kyle Kisor, Kevin Wilkins, Zoë Neckar, Natanya Kerper, Brian Tran, Tyler Pina, Dr. Andrew Mancini, Céline Mahieu, Dr. Aaron Mattingly, Dr. Kojo Opoku-Nsiah, Catherine Tan, Dror Assa, Dr. Darwin Mastin, Kathleen Mahoney, Jaclyn Scott, Ginger Westbrook, Elizabeth Irish, Dr. Christopher Bailey, the Cold Spring Harbor Laboratory Quantitative Imaging Course, and the HHMI Gilliam Fellows network.

Lastly, I am immeasurably grateful to my family. I cannot express enough what your love and support has meant to me before, during, and upon the completion of this major accomplishment. To my brother, Robby Robinson, and my newly-minted Doctor of Optometry '21 sister, Dr. Selena Aloisio, thank you both for always keeping me grounded and for making me so very proud to be your sister. To my partner, Marcus

Isaksson, whose serendipitous appearance in my life halfway through this degree completely changed everything. Thank you for keeping me sane and fed while I finished a PhD during a global pandemic. You're my coolest story, and I can't wait to keep on adding to it with you forever. Lastly, to my parents, Frank Aloisio and Jackie Aloisio, who have supported me in absolutely everything I've ever done. I love you so much, and I am forever grateful for your relentless support, nurturing love, and hearty laughter through it all. Un quiti xx

Contributions to this work

The work presented in this dissertation was performed under the supervision and guidance of Dr. Diane Barber, PhD. Additional guidance and insight were provided by thesis committee members Dr. Julie Sneddon, PhD, Dr. Todd Nystul, PhD, and Dr. Matthew Welch, PhD.

Chapter 2 of this work is adopted from a collaborative effort with Todd Nystul's lab as it appears in the following publication:
Tatapudy, S., **Aloisio, F.**, Barber, D., and Nystul, T. (2017). Cell fate decisions: emerging roles for metabolic signals and cell morphology. EMBO Rep *18(20)*, 2105-2118.

Chapter 3 of this work is adopted from efforts described in a manuscript which has been submitted for publication:
Aloisio, F., and Barber, D. (2021). Arp2/3 complex activity is necessary for mouse embryonic stem cell differentiation, times formative pluripotency, and enables lineage specification. *Manuscript submitted.*

Arp2/3 complex activity is necessary for mouse embryonic stem cell differentiation, times formative pluripotency, and enables lineage specification

Francesca M. Aloisio

Abstract

Mouse embryonic stem cells (mESCs), an *in vitro* model for naive pluripotent differentiation into primed pluripotent epiblast-like cells (EpiLCs), have been used to reveal transcriptional and epigenetic control of early embryonic development. However, the control and significance of morphological changes during lineage specification remain less defined. We show with quantitative time-lapse imaging marked changes in morphology and actin architectures during differentiation that depend on activity of the Arp2/3 complex, an actin filament nucleator. Inhibiting Arp2/3 complex activity pharmacologically or genetically does not block exit from naive pluripotency but attenuates increases in EpiLC markers compared with controls. We found that loss of Arp2/3 complex activity delays entry into the intermediate formative pluripotent state, resulting in globally defective lineage specification as indicated by RNA-sequencing with marked effects on TBX3-depedendent transcriptional programs. Further, we identified two previously unreported indicators of pluripotent status; MRTF and FHL2, which have inverse actin-dependent nuclear translocation as competing SRF co-factors that is dependent on Arp2/3 complex but not formin activity. These data reveal a previously unrecognized role for Arp2/3 complex-dependent actin remodeling in mESC differentiation, timing of formative pluripotency, and TBX3-dependent lineage

specification, as well as newly identified MRTF and FHL2 nuclear shuttling. Moreover, our current findings on a role for Arp2/3 complex activity in mESC differentiation compared with the established role for formin activity in epithelial to mesenchymal transition indicate that distinct actin nucleators regulate distinct modes of epithelial plasticity.

Table of Contents

List of Figures

List of Tables

CHAPTER 1: INTRODUCTION

Mouse embryonic stem cell differentiation

During *in vivo* early embryonic development, pluripotent stem cells comprise the inner cell mass of the early blastocyst that will ultimately give rise to each of the myriad cell types necessary to form the developing fetus. As an *in vitro* model, naive mouse embryonic stem cells (mESCs) derived from the inner cell mass have provided insights on the regulated transition to primed pluripotent epiblast-like cells (EpiLCs) of the post-implantation blastocyst (Martin, 1981; Evans and Kaufman, 1981), which is one of the earliest known transitions in embryonic differentiation (Nichols and Smith, 2009; Nichols and Smith, 2012; Weinberger et al., 2016). While *in vitro* studies with mESCs have revealed how biochemical cues, transcriptional programs, and epigenetics drive differentiation, less is known about morphological changes during differentiation, how they are controlled, and their importance for naive mESC differentiation or lineage specification (Gilmour et al., 2017; Villeneuve and Wickström, 2021).

Propagating clonal naive self-renewing mESCs requires maintenance in the presence of LIF2i (Leukemia Inhibitory Factor and pharmacological inhibitors for MEK and glycogen synthase kinase-3β) (Ying et al., 2008). Upon removal of LIF2i, mESCs spontaneously differentiate and transition through a formative pluripotency to a primed pluripotency state before lineage specification and commitment, recapitulating *in vivo* stages of early embryonic development. Formative pluripotency, a recently identified intermediate state during differentiation of naive mESCs to EpiLCs (Kalkan and Smith, 2014), is considered an executive phase when naive self-renewing signaling networks are dismantled and cells acquire competence for lineage specification. For example, OTX2

supports reorganizing gene regulatory networks with entry to formative pluripotency by recruiting OCT4 away from enhancers promoting naive self-renewal and toward enhancers for transcriptional programs related to lineage specification (Kalkan and Smith, 2014). In this way, formative pluripotency generates a population of intermediate cells with a uniformly heightened competence for responding to differentiation cues, which is distinct from naive cells in the presence of LIF2i that are shielded from differentiation and from primed cells that have initiated a biased differentiation response (Smith, 2017; Kalkan et al., 2019).

Increased understanding of the molecular foundation of formative pluripotent cells, which are responsive to differentiation cues and competent for lineage specification is critical for improving directed differentiation and for applications in regenerative medicine. A major limitation for a mechanistic understanding of formative pluripotency timing and regulation is the ambiguity of experimentally isolating and continuously propagating cells in this state (Smith, 2017; Kalkan et al., 2017; Mulas et al., 2017; Kinoshita and Smith, 2018). While recent findings suggest a cell culture method for capturing some aspects of formative pluripotency in mouse and human ESCs (Kinoshita et al., 2021), a clear understanding of what traits constitute a bona fide formative pluripotent stem cell remains unresolved. Further, there is disagreement on the *in vivo* timing for formative pluripotency, with some groups claiming that it occurs between E4.75-E5.75 (Kalkan et al., 2017) and others between E5.5-E6.5 (Morgani et al., 2017). It is commonly accepted, however, that formative pluripotency likely involves multiple effectors cooperating for a multilayered signaling network that ensures timely and robust

transition to this critical stage of embryonic lineage specification (Kalkan et al., 2019). Findings during my thesis research reveal a previously unrecognized role for the Arp2/3 complex in timing entry into formative pluripotency and subsequent lineage specification, which identifies new approaches for studying pluripotency transition states that could be applicable for regenerative medicine.

Arp2/3 complex activity-dependent actin remodeling

Actin remodeling is a major driver of morphological changes that facilitates diverse cell behaviors and structures such as lamellipodium, filopodium, endosomes, microvilli, ruffles, adherens junctions, and nuclear actin (May, 2001; Goley and Welch, 2006; Chhabra and Higgs, 2007). Actin filament architectures are predominantly generated by two classes of actin nucleators: the Arp2/3 complex comprising seven subunits that nucleates branched actin filaments, and formins, a family of fifteen mammalian isoforms that nucleate unbranched actin filaments. Each class of nucleators is regulated by distinct mechanisms in the context of discrete as well as common extracellular and intracellular chemical and mechanical cues and signals. These and other nucleators promote actin polymerization by overcoming the energetically unfavorable process of joining three G-actin monomers to initiate filament formation and elongation (Chhabra and Higgs, 2007).

Each of the seven subunits in the Arp2/3 complex play specific yet coordinated roles in nucleating branched actin filaments, including complex activity stimulation, nucleation, branching, and organizing (Welch et al., 1997; Gournier et al., 2001). The structure and

function of the Arp2/3 complex is evolutionarily conserved with high sequence similarity of the seven subunits across eukaryotes (Machesky et al., 1997; Welch et al., 1997). Activity of the Arp2/3 complex is tightly regulated as a coincidence detector with both phosphorylation of the Arp2 subunit and binding with a nucleation promoting factor (NPF) required to relieve autoinhibition (Robinson et al., 2001; Welch and Mullins, 2002; LeClaire et al., 2008). Another layer of Arp2/3 complex regulation arises from multiple branched actin filament inhibiting actin regulatory proteins such as coronin, cofilin, gadkin, arpin, GMF, and PICK1 (Burianek and Soderling, 2013; Swaney and Li, 2016; Sokolova et al., 2017). For example, Gadkin binds the Arp2/3 complex to inhibit cell spreading and motility (Maritzen et al., 2012) while arpin binds and inhibits the Arp2/3 complex in place of WAVE to steer directional migration downstream of Rac signaling (Dang et al., 2013).

With activity regulated by distinct mechanisms across diverse signaling networks and cellular contexts, the Arp2/3 complex exists as a robust molecular machine for a wide range of cellular processes. Activity of the Arp2/3 is critical for different modes of cell migration, including haptotaxis, durotaxis, and mechanotaxis (Devreotes and Horwitz, 2015) while also regulating tissue mechanics, including tension, contractility, and stiffness. In the context of development, contractility-regulated YAP and TAZ activity have noted roles in developmental transcriptional programming (Yoo et al., 2007; Olson and Nordheim, 2010; Dupont et al., 2011; Halder et al., 2012; Janmey et al., 2013). Further, force-sensitive lineage specification *in vivo* has been described in multiple organisms (Keller et al., 2003; Krieg et al., 2008; Gilmour et al., 2017; Villeneuve and

Wickström, 2021). Lastly, actin remodeling in the nucleus is reported to control transcription (Belin and Mullins, 2013; Hurst et al., 2019) and is sufficient to activate SRF target genes (Baarlink et al., 2013), osteogenic gene expression (Sen et al., 2015), and chromatin remodeling (Le et al., 2016). Arp2/3 complex-dependent branched actin networks serve a plethora of cellular functions as both interpreters and producers of biomechanical signals across several biochemical pathways (Papalazarou and Machesky, 2021).

Although Arp2/3 complex activity has not been reported for roles in pluripotency transition or lineage specification, processes it regulates, including cellular stiffness (Bongiorno et al., 2018), formation of ventral cortex F-actin asters (Xia et al., 2019), and dynamic membrane tension (De Belly et al, 2021; Bergert et al., 2021), have reported roles in mESC differentiation. My thesis research shows that during mESC differentiation morphological changes and actin filament remodeling are dependent on activity of the Arp2/3 complex but not formins, and that Arp2/3 complex activity is necessary for transition from naive mESCs to EpiLCs, including timing entry into intermediate formative pluripotency with global effects on lineage specification.

CHAPTER 2: ADHESION AND MORPHOLOGY DYNAMICS IN CELL FATE

Although differentiation often includes changes in cell shape and cell adhesion, including both cell–cell and cell-matrix adhesion, we have an incomplete understanding of how these changes are regulated during differentiation and contribute to the differentiation process. Understanding the underlying cell biology of differentiation, especially during in vivo development, requires knowledge of how the cell interprets its niche through cell shape and adhesion- derived mechanical forces. In this section, we review recent progress in how cell morphology and mechanical cues instruct cell fate decisions (**Fig. 2.1**).

Cell-substrate adhesion

Extracellular matrix (ECM) interactions with integrins and the changes in cell shape and tensional forces they generate provide instructive cues in stem cell fate decisions for both embryonic and adult stem cells, although downstream pathways result in divergent outcomes depending on the cellular context. Variable matrix elasticity directs MSC lineage specification with a greater selectivity than through biochemical cues and generates cellular fate memory that persists after cells are removed from a given matrix (Engler et al., 2006). Furthermore, pre-committing naive MSCs on a matrix stiffness that most closely recapitulates in vivo niche stiffness improves microenvironment adaptation upon implantation (Engler et al., 2006). The effect of cell shape on MSC fate decisions has also been shown by plating cells on small fibronectin islands, which reveals that cells with a rounded morphology differentiate to adipogenic lineages, while cells with a flattened cell shape differentiate to osteogenic lineages (McBeath et al., 2004). This morphology-driven differentiation is dependent on activity of the low molecular weight GTPase RhoA, indicating that the mechanical cues of cell shape and contractility

contribute to lineage commitment in MSCs. In support of this finding, McBeath and colleagues suggest that changes in cell shape sensed through integrin binding of ECM ligands, which provide tensional forces, can drive signaling cascades that result in altered gene expression in MSCs (McBeath et al., 2008).

In contrast to these MSCs that respond to integrin signaling with self-renewal, ECM–integrin interactions facilitate differentiation in mouse ESCs (Hayashi et al., 2007). Teasing apart the roles of mechanical forces resulting from integrin-mediated cell–ECM adhesion versus E-cadherin-mediated cell–cell adhesion, Uda et al. found that force via integrins but not E-cadherins decreases Oct3/4 expression in mouse ESCs (Uda et al., 2011), suggesting mechanical forces from distinct force transduction pathways can play divergent roles in embryonic stem cell biology.

Divergent roles for cadherin-mediated and integrin-mediated force transduction pathways may occur in the stem cell niches present in Drosophila melanogaster gonad development. DE-cadherin, the Drosophila melanogaster homolog of E-cadherin, mediates cell–cell adhesion between germline stem cells and other cells within the Drosophila ovary niche for both proper recruitment and anchoring (Song et al., 2002). Somatic stem cells within the Drosophila ovary generate follicle progenitor cells and several differentiated cells within the chamber. These epithelial stem cells are similarly anchored to the surrounding niche by DE-cadherin in order to prevent differentiation (Song and Xie, 2002). In addition to this cadherin-mediated cell–cell adhesion, integrins also enable follicle stem cells in the Drosophila ovary to adhere to surrounding basal lamina in the niche, anchoring them in position to respond to cues regulating their

differentiation (O'Reilly et al., 2008). During gonad morphogenesis in the Drosophila testis, germline stem cells contact hub cells in the niche. Integrin-dependent adhesion but not DE-cadherin-dependent adhesion positions the hub cells such that ECM surrounding the gonads anchors the niche and the germline stem cells (Tanentzapf et al., 2007; Voog et al., 2008). Somatic stem cells within the Drosophila testis must also contact hub cells to maintain self-renewal and proliferation, but these contacts are DE-cadherin- mediated (Voog et al., 2008). Though dependent on distinct anchoring mechanisms, positioning of both germline stem cells and somatic stem cells along hub cells within the Drosophila testis allows cooperation during gametogenesis as both cell types respond in different ways to local JAK-STAT signaling within the niche (Issigonis et al., 2009). A recent study suggests that DE-cadherin affects signaling in the Drosophila ISCs through a feedback loop that couples enterocyte cell death to ISC divisions (Liang et al., 2017). In this tissue, b-catenin is typically sequestered at the adherens junctions in enterocytes, but enterocyte cell death disrupts these junctions and thus causes the release of b-catenin. b-catenin then translocates to the nucleus where it activates the expression of rhomboid, which promotes the secretion of EGF ligands and ultimately leads to increased ISC proliferation.

We highlight here merely some advances in our understanding of how cell–ECM interactions and cell shape contribute to stem cell fate decisions. For more comprehensive discussions, we refer readers to reviews on ECM, integrins, and growth factors directing stem cell fate (Brizzi et al., 2012), nanoscale features of integrin–matrix interactions, matrix stiffness and 2D versus 3D cultures (Dalby et al., 2014), and integrin- and cadherin-mediated adhesion in maintaining a supportive niche for stem cell

anchoring, self-renewal, and differentiation (Raymond et al., 2009; Xi, 2009; Chen et al., 2013).

Cell–cell adhesion

The role of cadherin-mediated cell–cell adhesion in pluripotent cells is currently an area of active investigation. In mouse embryos, the adherens junction protein E-cadherin is highly expressed until gastrulation, when E-cadherin is downregulated as epithelial epiblasts undergo an epithelial-to-mesenchymal transition (EMT) and germ layers are specified. Animals null for E-cadherin are unable to complete embryogenesis beyond this point (Larue et al., 1994; Stephenson et al., 2010), which may be due in part to the lack of mechanical forces at adherens junctions (Zoldan et al., 2011). However, heterozygous loss of E-cadherin combined with N-cadherin knock-in results in normal embryonic development (Kan et al., 2007). Whether the in vivo role for E-cadherin is similar for differentiation of embryonic stem cells in vitro remains controversial. Spencer et al. found that mouse ESC differentiation involves traditional markers of EMT such as an E-cadherin to N-cadherin switching, increased expression of the E-cadherin repressors Snail and Slug, and increased cell motility (Spencer et al., 2007). Also in support of a pluripotent self-renewal promoting role for cell–cell adhesion, E-cadherin-mediated cell–cell contacts promote mouse ESC self-renewal and induced pluripotent stem cell (iPSC) generation (Chen et al., 2010; Bedzhov et al., 2013). In agreement with this proposed role, mouse ESCs null for E-cadherin have a transcriptional profile that more closely resembles differentiated epiblast stem cells than self- renewing naive ESCs (Soncin et al., 2011). Interestingly, genes most differentially expressed in self-renewing ESCs from E-cadherin$^{-/-}$ compared with WT mice are not limited to cell

adhesion and motility but also includes transcripts related to metabolic processes, catabolism, and apoptosis (Soncin et al., 2011). A comprehensive evaluation of the roles for E- cadherin in embryonic stem cells, pluripotency, and self-renewal is beyond the scope of our discussion of lesser-studied regulators of stem cell biology, but we refer the reader to several excellent reviews on this topic (Pieters and van Roy, 2014; Mohamet et al., 2011; Soncin and Ward, 2011).

Like E-cadherin, the role of b-catenin in stem cell self-renewal and differentiation is currently controversial, despite consensus on the importance of repressive transcriptional activity Tcf3 down- stream of canonical Wnt signaling, as described more completely in recent reviews on embryonic (Ying and Smith, 2017) and adult (Kretzschmar and Clevers, 2017) stem cells. For embryonic stem cells, conflicting findings may result from distinct b-catenin functions as an adherens junction protein and a signaling molecule in the Wnt pathway, with perhaps a cell–cell adhesion function being more critical. In brief, for embryonic stem cells, one view is that b-catenin is not necessary for the self-renewal and expansion of naive mESCs, but its absence eliminates the self-renewal response to Gsk3 inhibition (Wray et al., 2011). Another non-contradictory view is that a complex of b-catenin, E-cadherin and Oct 4 but not b-catenin transcriptional activity is necessary for pluripotency (Faunes et al., 2013). Additionally, b-catenin may be necessary for subsequent differentiation stages because mesendodermal germ layer formation and neuronal differentiation are defective in b-catenin-null mESCs (Lyashenko et al., 2011). Redundancy between catenins may also explain conflicting findings because in b-catenin-null mESCs, loss of c-catenin promotes exit from pluripotency (Mahendram et al., 2013), which further suggests the importance

of the adherens junctions but not signaling function of b-catenin in embryonic stem cell self-renewal and differentiation.

Actin filaments

Although actin filament dynamics regulate cell-substrate adhesion, cell–cell adhesion, and cell morphology, we have limited understanding of its direct role in stem cell differentiation and lineage specification. Moreover, how actin cytoskeleton dynamics might regulate transcriptional programs in cell differentiation is incompletely understood, although current evidence implicates roles for YAP, transcriptional activator with PDZ-binding motif (TAZ), and myocardin-related transcription factor (MRTF), which are transcriptional regulators responding to mechanical force or actin remodeling. YAP and TAZ, transcriptional cofactors in the Hippo signaling pathway, are both required for early mouse embryo development (Morin-Kensicki et al., 2006). In response to mechanical cues, YAP and TAZ translocate from the cytoplasm to the nucleus where they bind the transcription factor TEAD and other promoter-specific transcription factors (reviewed in Halder et al, 2012). Higher stiffness of the surrounding extracellular matrix results in nuclear YAP/TAZ localization by an unclear mechanism that senses cell tension (Dupont et al, 2011). Multiple types of mouse stem and progenitor cells, including ESCs, are characterized by upregulated YAP expression, suggesting that Hippo signaling promotes pluripotency-related pathways (Ramalho-Santos et al., 2002). Additionally, Yorkie, the Drosophila homolog of Yap, causes increased ISC proliferation in response to intestinal epithelia damage (Shaw et al., 2010; Staley et al., 2010) and also functions downstream of hedgehog signaling to promote proliferation of follicle stem cells (Huand and Kalderon, 2014). In the mouse intestine, Yap activity contributes to the

downregulation Wnt signaling, which is the key ISC self-renewal signal, and overexpression of Yap causes ISC loss whereas knockout of Yap causes an increase in the number of ISCs and Paneth cells. In contrast, overexpression of Yap in the epidermis has the opposite effect, causing an expansion of the stem cell pool and the formation of squamous cell-like carcinomas. However, knockout of the upstream negative regulator, Mst1/2, does not have the same effect, suggesting that Yap is activated by a non-canonical mechanism in this tissue.

Myocardin-related transcription factor is another link between actin remodeling and transcriptional regulation. In contrast to nuclear translocation of YAP/TAZ in response to cell-substrate signals, MRTF is translocated from the cytosol to the nucleus in response to increased actin polymerization (McGee et al., 2011; Miralles et al., 2003). In the nucleus, MRTF is a cofactor for transcriptional regulation by SRF to induce expression of over 200 transcripts, mostly related to actin dynamics, cell motility, muscle-specific genes, and miRNAs (reviewed in Olson and Nordheim, 2010). Although a role for MRTF in ESCs remains undetermined, it is important for adult MSC differentiation. Specifically, the degree of cell spreading in a precursor of the adipogenic and osteogenic lineages increases actin polymerization, and MRTF is translocated to the nucleus to promote osteogenic gene expression programs (Wang et al., 2002; Parmacek, 2007; Nobusue et al., 2014; McDonald et al., 2015; Bian et al., 2016).

Despite recent advances, further understanding of how cell shape, adhesion, and actin filament dynamics contribute to stem cell differentiation is needed to inform how directed in vitro differentiation protocols are optimized for regenerative medicine

applications. For example, Gilbert et al. showed that differentiating muscle cells reorganizes their actin cytoskeleton to match their cultured substrate stiffness, significantly improving the cell's ability to engraft and properly heal after implantation when the cultured substrate stiffness matched that of the in vivo niche (Gilbert et al., 2010). Additionally, Myers et al. found that cell colony geometry is a driver of stem cell fate decisions in 2D culture systems: patterning of colonies according to uniform size, density, and shape resulted in improved homogeneity and yield of human iPSC-derived cardiomyocytes (Myers et al., 2013). Zoldan et al. found that culturing hESCs on variable scaffold stiffnesses was sufficient to induce lineage-specific gene expression (Zoldan et al., 2011). As the field of regenerative medicine continues to develop in vitro-derived cell replacement therapeutics, knowledge of the underlying cell biology of stem cell shape and adhesion as it pertains to both in vivo development and in vitro differentiation will greatly inform future studies.

Figures

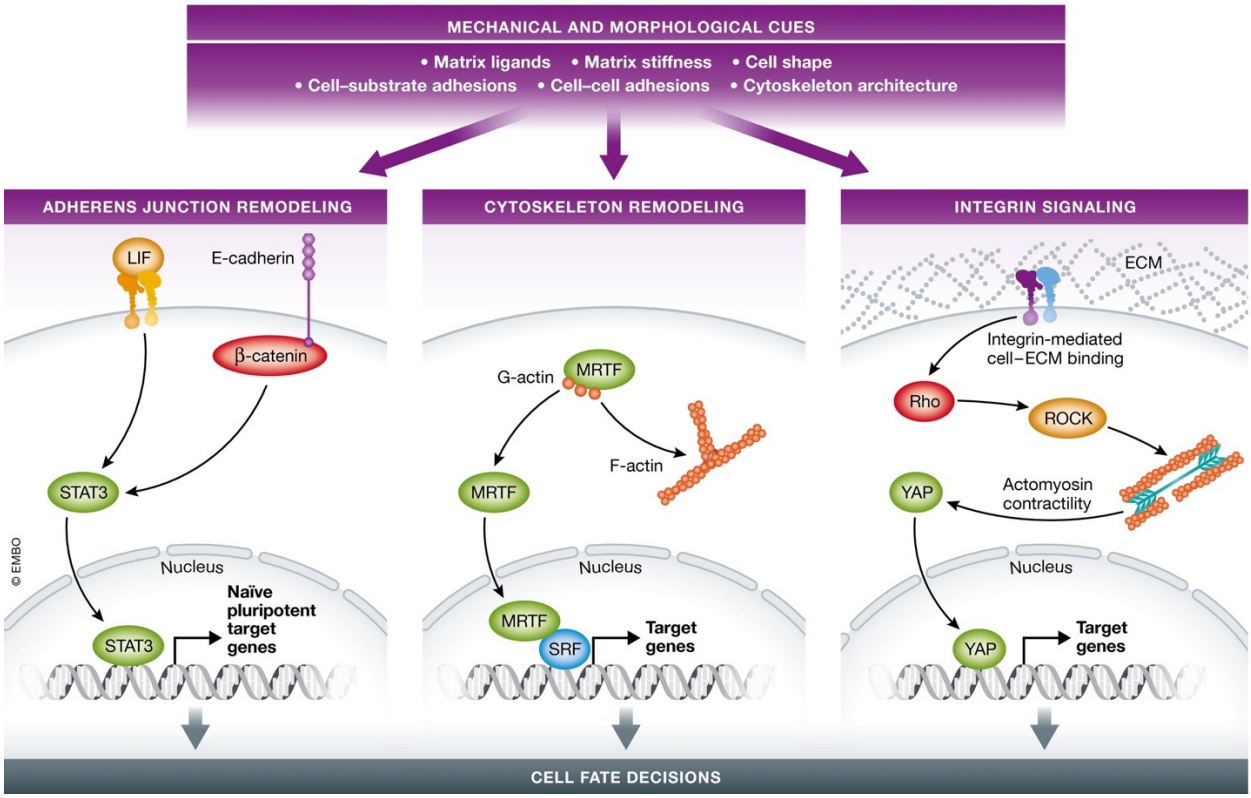

Figure 2.1: Mechanical and morphological cues regulate cell fate decisions through distinct signaling mechanisms.

Cues provided by extracellular matrix (ECM) ligands, ECM stiffness, cell shape, cell-substrate adhesion, cell-cell adhesion, and cytoskeleton architectures inform the cell of its surrounding niche (right panel). The naive state of clonal embryonic stem cells is routinely maintained in medium supplemented with leukemia inhibitory factor (LIF), which activates STAT3 to induce expression of naive pluripotent target genes. However, expression of E-cadherin in pluripotent stem cells is sufficient to promote LIF-independent self-renewal by activating STAT3 to induce expression of naive pluripotent target genes. This later effect requires the b-catenin-binding region of E-cadherin (left panel). With increased actin polymerization, myocardin-related transcription factor (MRTF), which is retained in the cytoplasm by binding to G-actin, translocates to the nucleus where it binds the transcription factor serum response factor (SRF) to activate genes regulating differentiation programs (middle panel). In response to integrin-mediated cell-substrate adhesion, the low molecular weight GTPase Rho activates Rho-associated protein kinase (ROCK) to generate actomyosin contractility, which results in nuclear translocation of yes-associated protein (YAP) (right panel).

CHAPTER 3: ARP2/3 COMPLEX ACTIVITY IS NECESSARY FOR MOUSE ESC DIFFERENTIATION, TIMES FORMATIVE PLURIPOTENCY, AND ENABLES LINEAGE SPECIFICATION

Inhibiting Arp2/3 complex but not formin activity blocks morphological changes and actin remodeling during mESC differentiation

A mechanism for changes in mESC morphology by actin remodeling and how they are regulated in the context of differentiation and lineage specification remains incompletely understood. Recent advances proposed roles for dynamic cell membrane tension and polarity as requisite regulators of both *in vitro* mESC differentiation (Xia et al., 2019; Bergert et al., 2021) and *in vivo* embryonic development (Molé et al., 2021); however, to our knowledge a direct link between actin-dependent changes in morphology and the transcriptional programming of lineage specification has not been reported. To quantify changes in mESC colony morphology in real time we used quantitative DIC imaging of naive E14 mESCs maintained in the presence of LIF2i (Leukemia Inhibitory Factor and pharmacological inhibitors PD03259010 for MEK and CHIR99021 for glycogen synthase kinase-3β) and spontaneously differentiated for 72h after removal of LIF2i (Ying et al., 2008). Naive colonies in LIF2i have a static circular morphology as quantified using *circularity = 4pi(area/perimeter^2)* with a value of 1.0 indicating a perfect circle and values approaching 0.0 indicating an elongated polygon shape (**Fig. 3.1A-B, Movie 1**). In control cells, colony circularity progressively decreases at 24h, 48h and 72h after removing LIF2i (**Fig. 3.1B, Movie 2**). Similar morphological changes during mESC differentiation were recently reported (Bongiorno et al., 2018; Bergert et al., 2021); however, a regulatory mechanism for dynamic cell and colony morphology was not identified. In determining how these morphological changes are regulated we find that decreases in colony circularity at 48h and 72h -LIF2i are significantly attenuated by CK666, a selective pharmacological inhibitor of Arp2/3 complex activity

(Nolen et al., 2009; Yang et al., 2012) but not by SMIFH2, a broad-spectrum inhibitor of formin activity (Rizvi et al., 2009; Ganguly et al., 2015) (**Fig. 3.1A-B**). In contrast, we recently showed that SMIFH2 but not CK666 blocks morphological changes during epithelial to mesenchymal transition (EMT) (Rana et al., 2018). Although the selectivity of SMIFH2 was recently shown to also include non-muscle myosins (Nishimura et al., 2021), its ability to inhibit formin activity remains undisputed. Hence, our current findings indicate that the Arp2/3 complex and formins have distinct roles in morphological changes during two different programs of epithelial plasticity, mESC differentiation and EMT, respectively.

With the established role of Arp2/3 complex in nucleating branched actin filaments, we analyzed actin architectures during differentiation. Using high resolution spinning disc confocal imaging of phalloidin-labeled actin filaments we find that naive E14 mESCs in LIF2i have a compact polygonal cell shape with a cortical ring of straight actin filaments that are remodeled to an elongated cell shape with prominent membrane protrusions containing ribbed, fan-like actin filaments after 72h -LIF2i (**Fig. 3.1C**). In the presence of CK666 but not SMIFH2 actin filaments retain a cortical ring after 72h -LIF2i and fan-like filament networks are rarely seen (**Fig. 3.1C**). We also find that effects with CK666 are phenocopied with CRISPR/Cas9 knockdown of ARPC2, an Arp2/3 complex subunit. We confirmed CRISPR/Cas9 editing of the *Arpc2* locus by decreased ARPC2 in E14 mESCs by immunoblotting (**Fig. 3.7A-B**) and by sequencing (**Fig. 3.7E-F**). Consistent with the stability of Arp2/3 complex subunits being dependent on their assembly (Di Nardo et al., 2005; Steffen et al., 2006; Rauhala et al., 2013; LeClaire et al., 2015), with

Arpc2 silencing in mESCs there is significantly decreased abundance of the Arp2/3 complex subunit ARP2 (**Fig. 3.7C-D**). Inhibiting Arp2/3 complex activity in E14 mESCs by either CK666 or Arpc2 knockdown has no effect on the morphology or cortical actin organization of naive cells, but blocks pronounced fan-like actin filaments seen in membrane protrusions after 72h -LIF2i in control E14 cells (**Fig. 3.1C**). Similar to our findings with E14 mESCs, we confirmed that genetically distinct V6.5 mESCs show a similar remodeling of actin filament architectures with spontaneous differentiation that is blocked by CK666 but not SMIFH2 (**Fig. 3.1D**). Taken together, these findings indicate that actin remodeling with distinct changes in filament architectures occur during mESC differentiation in two mESC lines that are blocked by inhibiting Arp2/3 complex but not formin activity.

Changes in cell morphology are often not driven by actin filament remodeling alone but also in combination with actomyosin contractility (Murrell et al., 2015). In human induced pluripotent cells (iPSCs), a contractile actin fence promotes pluripotency and in mouse embryos suppressing actomyosin contractility regulates epiblast morphogenesis during pre- to post-implantation (Närvä et al., 2017; Molé et al., 2021). Consistent with our finding that CK666 attenuates changes in mESC colony morphology, immunolabeling indicates that phosphorylated MLC (pMLC), an indicator of actomyosin contractility, decorates the cortical actin ring around cells and the peripheral ring around free margins of colonies in control naïve mESCs but is diffuse in the cytoplasm after 72h -LIF2i (**Fig. 3.1G**). In contrast, in the presence of CK666 but not SMIFH2 pMLC retains a cortical localization after 72h -LIF2i (**Fig. 3.1G**). However, there is no change in pMLC

abundance during differentiation in controls or with CK666 or SMIFH2, determined by immunoblotting of E14 mESC lysates (**Fig. 3.7G-H**). Taken together, these data indicate that activity of the Arp2/3 complex but not formins regulates changes in colony morphology, actin architectures, and localized actomyosin contractility during mESC differentiation.

Inhibiting Arp2/3 complex but not formin activity impairs differentiation to EpiLCs

We used several approaches to show that Arp2/3 complex activity is also necessary for transcriptional changes during mESC differentiation**.** We first used a V6.5 dual-reporter (DR) mESC line engineered to express distinct fluorophores as cells transition from naive to primed pluripotency. In brief, work by Parchem et al. (2014) found that V6.5 mESCs in LIF2i express a naive-specific *miR-290* cluster and with spontaneous differentiation upon removal of LIF2i *miR-290* expression decreases and expression of the primed-specific *miR-302* cluster increases. They generated cells that express mCherry driven by the *miR-290* promoter and GFP driven by the *miR-302* promoter. Using flow cytometry, DR mESCs can be used to score for decreased mCherry expression and increased GFP expression as an index of differentiation on the cell population level, while intermediate cells are double-positive for both markers (**Fig. 3.2A**). Our analysis indicates that control DR mESCs in LIF2i are >90% mCherry positive (**Fig. 3.8A**), which is reduced to 16.3% after 72h -LIF2i in controls but is significantly greater at 44.0% with CK666 (**Fig. 3.2B**). In contrast, the percent of mCherry single-positive cells is not different with CK689, an inactive analog of CK666 (Nolen et al., 2009), the formin inhibitor SMIFH2, or DMSO as a vehicle compared with

controls (**Fig. 3.2A**). Further, cell death and proliferation in the presence of CK666, CK689, SMIFH2 or DMSO are not significantly different from control cells at any timepoint during differentiation (**Fig 3.8B, 3.8E**). These data indicate that Arp2/3 complex but not formin activity is necessary for changes in stage-specific miRNA expression during naive to primed pluripotency, suggesting a broader role for Arp2/3 complex-dependent actin remodeling in the context of mESC differentiation beyond changes in morphology.

As a second approach to test differentiation, we confirmed that CK666 and *Arpc2* silencing attenuates expression of established primed EpiLC markers. RT-qPCR for *Fgf5* (**Fig. 3.2C**) and *Brachyury* (**Fig. 3.2D**) in V6.5 DR mESCs indicates significantly increased expression in controls and with CK689 after 72h -LIF2i but not with CK666. We used a similar approach to show that expression of *Fgf5* in E14 mESCs significantly increases after 72h -LIF2i in controls but is attenuated with *Arpc2* silencing (**Fig. 3.2E**). These data support a role for Arp2/3 complex activity in transcriptional changes associated with differentiation of naive to primed EpiLCs as indicated by pharmacologically or genetically inhibiting Arp2/3 complex activity in V6.5 and E14 mESCs.

Our third approach to test differentiation scored for the cytosolic and nuclear localization TFE3, a bHLH transcription factor that is predominantly nuclear in naive mESCs but mostly cytoplasmic in primed EpiLCs (Betschinger et al., 2013; Villegas et al., 2019; Kalkan et al., 2017). Using quantitative immunolabeling of E14 mESCs, we see that the

nuclear to cytoplasmic ratio of endogenous TFE3 significantly decreases after 72h -LIF2i in controls but not in the presence of CK666 (**Fig. 3.2F-G**). Taken together, these data reveal a role for Arp2/3 complex activity beyond morphology to include transcriptional indicators such as miRNA expression, primed marker gene expression, and transcription factor localization during transition of naive mESCs to primed EpiLCs.

Inhibiting Arp2/3 complex activity has no effect on exit from naïve self-renewal but delays entry into formative pluripotency

To further understand how Arp2/3 complex activity enables mESC differentiation, we tested whether it is necessary for exit from naive pluripotency. At 72h -LIF2i, the naive marker *Rex1* (also called *Zfp42*) significantly decreases in V6.5 and E14 cells in the absence and presence of CK666 and CK689 (**Fig. 3.3A-B**) as well as in E14 cells with *Arpc2* silencing (**Fig. 3.3B**). Moreover, the time-dependent decrease in the expression of *Rex1* as well as *Stra8*, an additional naive marker, over 120h -LIF2i in E14 cells is similar in the absence or presence of CK666 (**Fig. 3.3C, Fig. 3.8F**). These data suggest that although Arp2/3 complex activity is necessary for increased primed EpiLC markers seen in controls, it is not necessary for maintaining naive markers or for exit from naive pluripotency.

An intermediate state between naive and primed pluripotency, termed formative pluripotency, was recently identified. Formative pluripotency is considered an "executive" state when cells are most responsive to differentiation cues and most receptive for lineage commitment (Smith, 2017; Kalkan et al., 2017; Kalkan et al., 2019).

Given our findings that inhibiting Arp2/3 complex activity has no effect on exit from naïve pluripotency but attenuates markers of primed pluripotency, we tested whether inhibiting Arp2/3 complex affects expression of intermediate formative pluripotent markers. The formative pluripotent state is currently defined by decreased expression of *Rex1*, which we confirmed is not impaired when Arp2/3 activity is inhibited (**Fig. 3.3A-C**), increased *Otx2* (Kalkan et al., 2017; Mulas et al., 2017), increased phosphorylated ERK (pERK) (Kalkan et al., 2019), and increased *Grhl2* (Chen et al., 2018). We confirmed that *Otx2* significantly increases in control E14 cells within 24h -LIF2i (**Fig. 3.3D**). In contrast, with CK666 *Otx2* expression at 24h -LIF2i is significantly less compared with control cells and not different than in naive cells (**Fig. 3.3D**). After 48h -LIF2i, however, CK666-treated cells have a delayed increase in *Otx2* (**Fig. 3.3D**). These results are temporally consistent both with the delayed decrease in colony morphology observed in CK666-treated E14 cells at 48h -LIF2i (**Fig. 3.1A-B**) and with previous reports for delayed *Otx2* expression at 48h -LIF2i in the presence of a pharmacological inhibitor of NODAL signaling, which is suggested to function as a timing mechanism for pluripotency transition (Mulas et al., 2017).

Increased pERK, another marker of formative pluripotency, is required for activating downstream formative pluripotent gene regulatory networks (Kalkan et al., 2019; Azami et al., 2019). We find increased pERK in control E14 cells at 24 and 48h -LIF2i compared with total ERK, which does not change during differentiation, as determined by immunoblotting cell lysates (**Fig. 3.3E-F**). In contrast, with CK666 pERK does not increase in -LIF2i cells compared with naive cells (**Fig. 3.3E-F**). We also used

immunoblotting of E14 cell lysates to confirm increased abundance of GRHL2 in control E14 cells at 24 and 48h -LIF2i (**Fig. 3.3G-H**), which is similar to reported findings using V6.5 cells (Chen et al., 2018). In contrast, with CK666 increased GRHL2 is delayed with a significant increase at 48h but not at 24h in -LIF2i in cells (**Fig. 3.3G-H**). Further, expression of *Cldn6*, a downstream target gene of GRHL2 in mESCs, significantly increases in control E14 cells at 24h -LIF2i but not with CK666 (**Fig. 3.3I**). Hence, inhibiting Arp2/3 complex activity in two different mESC lines has no effect on maintenance of naive self-renewal or exit from naive pluripotency but delays entry into the intermediate formative pluripotent state as indicated by attenuated *Otx2* and *Cldn6* expression as well as pERK and Grhl2 abundance.

Inhibiting Arp2/3 complex activity disrupts lineage commitment with pronounced effects on TBX3 target genes across all three germ layers

Our findings that Arp2/3 complex activity is necessary for actin remodeling, attenuated expression of primed marker expression, and timing for formative pluripotency during mESC differentiation suggest a role in promoting primed EpiLC lineage specification. To investigate global effects of inhibiting Arp2/3 complex activity on lineage specification, we performed RNA sequencing (RNA-seq) on E14 cells differentiated in the absence and presence of CK666 for 72h -LIF2i and control naive cells maintained in LIF2i (**Fig. 3.4A-B**). We found that control naïve +LIF2i and -LIF2i cells have a total of 6,576 differentially expressed genes (DEGs) with an adjusted qval < 0.05 after batch correction (**Fig. 3.4C**). Of these DEGs, 1,662 are unique to control -LIF2i cells compared with naïve +LIF2i cells and are not differentially expressed in CK666 -LIF2i

compared with naïve +LIF2i cells (**Fig. 3.4C**). CK666 -LIF2i cells compared with naïve +LIF2i have 4,796 DEGs, with 457 unique DEGs (**Fig. 3.4C**). In CK666 -LIF2i cells compared with both control +/-LIF2i cells, 972 unique DEGs are displayed (**Fig. 3.4A**). Gene Ontology (GO) enrichment analysis of this latter subset suggests that unique CK666-specific DEGs are associated with biological processes related to extracellular matrix organization, endothelial cell migration, sprouting angiogenesis, and the MAPK/ERK cascade (**Fig. 3.4D**). As a general summary, these data indicate global transcriptomic differences in naive +LIF2i cells, control -LIF2i cells, and CK666-treated -LIF2i cells.

Consistent with our data indicating that CK666 has no effect on exit from naïve self-renewal (**Fig. 3.3A-C**), RNA-seq data also show downregulated naive markers in the presence of CK666 compared with control cells with the exception of *Tbx3* (**Fig. 3.4E**). TBX3 is a master regulatory transcription factor known to play dual inhibitory and activating roles as mESCs transition from naive self-renewal to lineage specification (Lu et al., 2011; Kalkan et al., 2019). Consistent with significantly attenuated *Tbx3* expression in CK666 -LIF2i, a number of TBX3 target genes (Russell et al., 2015; Nishiyama et al., 2013; Han et al., 2010) such as *Fgf5*, *Fn1*, *Zeb1*, *Kctd12b*, and *Mat2a* (Fig. 4B) and targets specific to mesoderm such as *Pdlim3*, *Adm*, and *Fhl2*, (Fig. 4F), endoderm such as *Eomes* and *Kit*, (**Fig. 3.4G**), and ectoderm such as *Mycn*, *Prickle1*, and *Nes* (**Fig. 3.4H**) are significantly dysregulated. Taken together, these data indicate a role for Arp2/3 complex activity in timing of formative pluripotent lineage specification related to delayed extinction of naive-promoting targets of *Tbx3*, which is suggested to

counteract the initiation of formative pluripotent gene regulatory networks (Kalkan et al., 2019).

TBX3 is an established regulator of early development with dynamic context-dependent roles in embryonic organogenesis across germ layers (Chapman et al., 1996). With its binding to a number of transcription factors such as Klf4, Oct4, Sox2, and Nanog, TBX3 plays a complex role at the center of pluripotency circuitry (Han et al., 2010; Russell et al., 2015) with the potential to act as either an activator or inhibitor of gene expression dependent upon cofactor binding (Carlson et al., 2001). To determine the extent to which inhibiting Arp2/3 complex activity globally affects TBX3 target gene expression, we compared our DEGs to three publicly available mESC datasets related to target genes that change expression relative to a TBX3 reporter (**Fig. 3.5A**) (Russell et al., 2015), change expression with shRNA knockdown of *Tbx3* (**Fig. 3.5B**) (Nishiyama et al., 2013), and bind TBX3 as indicated by ChIP-sequencing (**Fig. 3.5C**) (Han et al., 2010). Comparing data sets shows that CK666 treatment during differentiation generally causes TBX3 target genes to have a contrasting transcriptional profile compared with that of a control differentiation: for each TBX3 gene list, our clustermaps indicate that genes with increasing expression in control -LIF2i had attenuated expression with CK666 and genes with decreasing expression in control -LIF2i had heightened expression with CK666 (**Fig. 3.5A-C**). Enriching for TBX3 target genes common to all three datasets that are significantly dysregulated with CK666 compared with control (**Fig. 3.5D**) suggests effects on a number of key regulators such *Mycn,* which is essential for neurogenesis (Knoepfler et al., 2002; Kerosuo et al., 2018), *Prdm1,* which

has multiple roles in neural fate and germ cell specification (Prajapati et al., 2019; Ohinata et al., 2005), and *Cobl*, which has an actin-related role in neural tube formation (Carroll et al., 2003). Other noteworthy gene expression changes include *Tfe3* (**Fig. 3.2F-G, Fig. 3.5A**) and *Cldn6* (**Fig. 3.3I, Fig. 3.5A**). Additionally, *Eomes*, a TBX3 target gene that plays a context-dependent role in specification of all three germ layers (Costello et al., 2011; Tosic et al., 2019) and *Fhl2*, a mesodermal marker and recently identified tension-dependent actin-binding protein (Sun et al., 2021), are significantly attenuated in the presence of CK666 (**Fig. 3.4F, 3.5A**). Collectively, these data suggest that Arp2/3 complex activity times entry into formative pluripotency, possibly by delayed loss of *Tbx3* expression, resulting in defective downstream global and distinct lineage specification programs.

Inhibiting Arp2/3 complex activity blocks cytoplasmic and nuclear shuttling of MRTF and FHL2

Our findings on TBX3 target genes regulated by Arp2/3 complex activity led us to identify two previously unreported markers of mESC differentiation – the cytoplasmic and nuclear localization of SRF co-transcriptional activators FHL2 and MRTF. MRTF is an actin polymerization-responsive transcriptional co-activator that, with increased actin polymerization, translocates to the nucleus (Miralles et al., 2003; Posern and Treisman, 2006). FHL2 is a TBX3 target gene and a transcriptional co-activator that is predominantly nuclear in response to decreased F-actin tension (Philippar et al., 2004; Nakazawa et al., 2016). Although formin-dependent nuclear translocation of MRTF is well-described for adult mesenchymal stem cell differentiation, neither MRTF nor FHL2

translocation has been reported to be regulated by Arp2/3 complex activity nor to translocate during mESC differentiation.

We scored for changes in MRTF localization during mESC differentiation and found that in control and SMIFH2-treated naive E14 cells MRTF is diffuse in the cytoplasm but after 72h -LIF2i becomes predominantly nuclear as quantified by a significant increase in the nuclear to cytoplasmic ratio (**Fig. 3.6A, B**). In contrast, with CK666 nuclear translocation of MRTF is inhibited with no increase in nuclear abundance at both 72h -LIF2i (**Fig. 3.6A, B**) and at 120h -LIF2i (**Fig. 3.9A, B**). These data indicate that MRTF nuclear translocation occurs during mESC differentiation and is dependent on activity of the Arp2/3 complex but not formins. Further, our RNA-seq data confirm that MRTF target genes (Esnault et al., 2014) have a contrasting transcriptional profile with CK666 compared to controls: our clustermap indicates that MRTF target genes going up in control -LIF2i had attenuated expression with CK666 and genes going down in in control -LIF2i had heightened expression with CK666, including *Fhl2* and *Srf* (**Fig. 3.6C**).

Similar to MRTF, nuclear FHL2 binds with transcription factor SRF to promote target gene expression with noted functions in mesoderm tissues (Lorda-Diez et al., 2018; Renger et al., 2013; Esnault et al., 2014; Philippar et al., 2004; Russell et al., 2015). We scored for changes in FHL2 localization during mESC differentiation and found that in control naive E14 cells FHL2 is nuclear but after 72h -LIF2i undergoes translocation to the cytoplasm, quantified by a significant decrease in the nuclear to cytoplasmic ratio

(**Fig. 3.6D, E**). In contrast, with CK666 cytoplasmic translocation of FHL2 is attenuated with no significant decrease in nuclear abundance at 72h -LIF2i (**Fig. 3.6D, E**). Taken together, these data reveal three previously unrecognized events during mESC differentiation; first is changes in the localization of MRTF and FHL2, second is the opposing nuclear and cytoplasmic translocation of these SRF transcriptional co-activators, and third is that their translocation is dependent on Arp2/3 complex activity (**Fig. 3.6F**).

Discussion

We report a previously unrecognized function of Arp2/3 complex activity in enabling the differentiation of naive to primed mESCs. We find that changes in colony morphology and actin architectures in mESCs are dependent on activity of the Arp2/3 complex but not formins. Our data also indicate that Arp2/3 complex activity is necessary for transition to distinct pluripotency states: although not necessary for exit from the naive state, loss of Arp2/3 complex activity delays entry into the formative pluripotent state, contributing further mechanistic insight on how this newly identified intermediate state is controlled (Smith, 2017; Kalkan et al., 2017; Kalkan et al., 2019). Further, our data include a global examination of actin-dependent lineage specification across all three germ layers in mESCs, which align with evolutionarily conserved roles for force-sensitive differentiation and development in other organisms both and *in vitro* (Chowdhury et al., 2010; Lee et al., 2013) and *in vivo* (Keller et al., 2003; Krieg et al., 2008). Lastly, we show for the first time that MRTF and FHL2, both actin-responsive

transcriptional co-activators to SRF, undergo inverse Arp2/3 complex activity-dependent translocation events during mESC differentiation.

We show marked changes in colony morphology and actin architectures during differentiation that depend on Arp2/3 complex but not formin activity. These findings are consistent with reported observations related to morphology and dynamic cellular stiffness during differentiation (Bongiorno et al., 2018) and an acute role for the Arp2/3 complex in mESC actin remodeling (Xia et al., 2019). We observed Arp2/3 complex-dependent actin architectures, which are estabished to generate generate protrusive forces for membrane dynamics (Bailly et al., 2001; Swaney and Li, 2016) and is of particular interest with regard to recently reported roles for dynamic membrane tension related to cortical actin detachment during mESC pluripotency transition (Bergert et al., 2021; De Belly et al., 2021). An important question to resolve is how Arp2/3 complex activity regulates transcriptional changes in mESCs compared with its regulation of transcriptional events in other cell models (Yoo et al., 2007; Olson and Nordheim, 2010). Previous studies have indicated force-sensitive lineage specification (Keller et al., 2003; Krieg et al., 2008; Gilmour et al., 2017; Villeneuve and Wickström, 2021) as well as mechanosensing and contractility in fate specification for mESCs (Janmey et al., 2013; Happe and Engler, 2016; Tatapudy et al., 2017). The role of Arp2/3 complex as a central node between biochemical cues and biophysical responses (Iskratsch et al., 2014; Charras and Yap, 2018) suggests a mechanosensitive mechanism whereby Arp2/3 complex activity enables mESC differentiation.

Our data also suggest that Arp2/3 complex activity times entry to intermediate formative pluripotency, an “executive” state when cells are most receptive for lineage specification cues (Smith, 2017; Kalkan et al., 2017; Kalkan et al., 2019). Inhibiting Arp2/3 complex activity delays entry into formative pluripotency, as indicated by the delayed increase in *Otx2* and *Cldn6* expression, and GRHL2 abundance as well as no change in pERK with -LIF2i compared with controls. In related findings, inhibiting NODAL signaling has no effect on exit from naive pluripotency but delays formative pluripotent marker expression from 24h to 48h -LIF2i (Mulas et al., 2017). Taken together, our data indicate that Arp2/3 complex activity is a previously unrecognized node in the growing signaling network of formative pluripotent regulators, which adds mechanistic insight relevant to embryonic lineage specification.

We also reveal that inhibiting Arp2/3 complex activity disrupts lineage commitment across all three germ layers with pronounced effects in TBX3 target genes compared with control cells. TBX3 is a context-dependent master regulator of both naive self-renewal (Niwa et al., 2009; Han et al., 2010; Russell et al., 2015) and lineage specification (Costello et al., 2011; Lu et al., 2011; Weidgang et al., 2013; Kartikasari et al., 2013) and its continued expression during mESC differentiation is reported to destabilize entry into formative pluripotency (Kalkan et al., 2019). Dysregulated *Tbx3* expression is associated with atypical cell and colony morphology in mESCs (Han et al., 2010; Russell et al., 2015), which we also see with loss of Arp2/3 complex activity. Smith and colleagues proposed a relationship between timing of formative pluripotency and RBPJ, a regulator of mESC morphology, whereby RBPJ inhibits TBX3 expression

to block formative cells from returning to self-renewal (Kalkan et al., 2019). Further, ERK signaling is reported to inhibit *Tbx3* expression and mESCs null for ERK pathway components have sustained *Tbx3* expression (Niwa et al., 2009; Hamilton et al., 2013; Chen et al., 2015). Our data indicating attenuated pERK and persistent *Tbx3* abundance with CK666 suggest a relationship between Arp2/3 complex activity, mESC morphology, formative pluripotency and TBX3-dependent lineage specification. Future studies on the link between Arp2/3 complex activity and formative pluripotency timing will be important to resolve the interface between morphology and lineage specification, with potential relevance to enhanced protocols for directed differentiation.

We also show that MRTF and FHL2, actin-responsive transcriptional co-activators for SRF, undergo previously unreported translocation events during mESC differentiation. MRTF is a transcriptional co-activator SRF (Posern and Treisman, 2006; Sun et al., 2006; Vartiainen et al., 2007). With increased actin polymerization, MRTF translocates from the cytoplasm to the nucleus where it binds to SRF to promote differentiation programs in adult mesenchymal stem cells (Miralles et al., 2003; Nobusue et al., 2014; McDonald et al., 2015; Bian et al., 2016). Our data show two previously unreported findings on MRTF nuclear translocation; first that it occurs with mESC differentiation and second that it is dependent on Arp2/3 complex activity. Although MRTF has not been reported for direct roles in embryonic differentiation, SRF is confirmed to regulate embryonic mesoderm formation (Weinhold et al., 2000) and *Srf* -/- ESCs have altered cell morphology and reduced cortical actin (Schratt et al., 2002). FHL2, dysregulated in many cancers and developmental disorders, is another SRF-binding transcriptional co-

activator which exhibits a direct transcriptional response to the actin cytoskeleton (Sun et al., 2020) and is a TBX3 target gene (Russell et al., 2015). In the cytosol, FHL2 contains LIM domains that mechanoaccumulate on strain sites of tensed actin filaments (Sun et al., 2020). FHL2 is released from F-actin upon loss of filament strain, causing it to translocate to the nucleus where it competes with MRTF for SRF-binding (Philippar et al., 2004). In tandem, MRTF and FHL2 are both direct actin-responsive transcriptional co-activators with dueling roles both in the cytosol and in the nucleus: in the cytosol competing for actin-binding and in the nucleus competing for SRF-binding to promote distinct transcriptional programs. Our data show a previously unreported inverse translocation of MRTF and FHL2 with mESC differentiation. Taken together, these data suggest that inversely mechanosensitive translocation events of MRTF and FHL2 could serve as a novel marker for pluripotency status and provide motivation for understanding how basic cell biology such as actin remodeling can provide a framework for elucidating mechanisms of mESC differentiation and lineage specification.

As recently indicated (Gilmour, 2017; Villeneuve and Wickström, 2021), a current challenge is to identify the connection between the cellular machines that generate shape and the genes that control cell-fate decisions. Our observations, compared with previous findings that activity of formins but not Arp2/3 complex is necessary for EMT and the assembly of unbranched contractile actin filaments (Li et al., 2010; Jurmeister et al., 2012; Rana et al., 2018), indicate that these different classes of actin nucleators and the architectures they generate have selective roles in distinct types of epithelial plasticity. With known functions in migration (Suraneni et al., 2012; Arnold 2008) and

adherens junction tension (Verma et al., 2012; Fierro-Gonzales et al., 2012), there are abundant potential mechanisms whereby Arp2/3 complex activity might regulate mESC pluripotency transition (Rotty et al., 2013; Pieters and van Roy, 2014; Wagh et al., 2021; Molé et al., 2021). Our study provides a step toward closing the gap between phenotype and genotype, opening new directions and advancing new approaches to understand how morphological changes and actin filament dynamics promote pluripotency transition, with potential value for additional approaches in directing differentiations for regenerative medicine.

Acknowledgments

We thank A. Smith (University of Cambridge) for providing the E14 cell line and R. Blelloch (UCSF) for providing V6.5 wild type and DR cells. We also thank T. Nystul (UCSF), M. Welch (UC Berkeley), and the Barber Lab for helpful discussions. This work was supported by NIH grants GM116384 and CA197855 to DLB. FMA was supported by an HHMI Gilliam Fellowship, a UCSF Moritz-Heyman Discovery Fellowship, and an NIGMS T32GM008568 training grant.

Figures

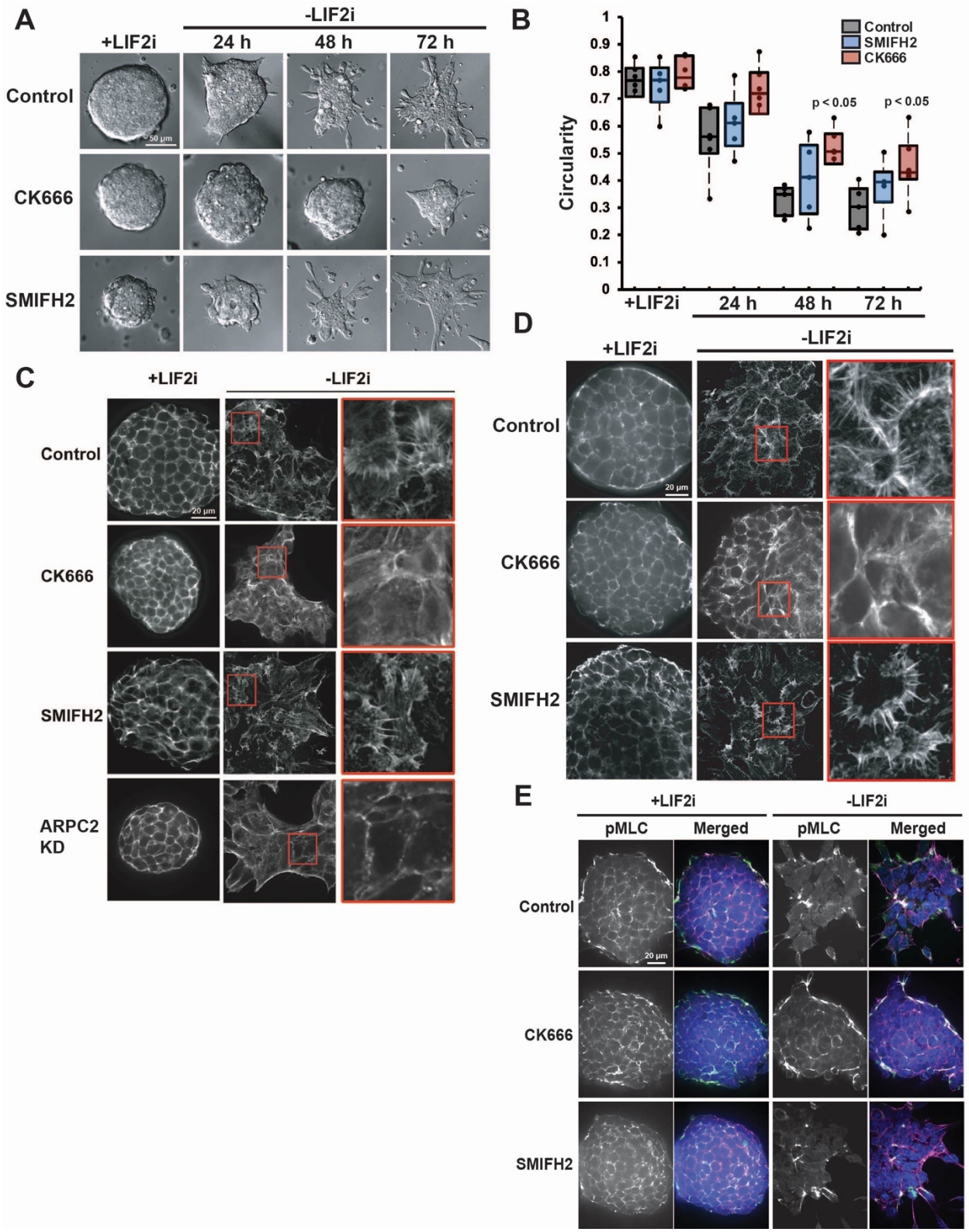
A
-LIF2i
+LIF2i
24 h
48 h
72 h
Control
CK666
SMIFH2
50 µm
B
Control
SMIFH2
CK666
Circularity
p < 0.05
p < 0.05
+LIF2i
24 h
48 h
72 h
C
+LIF2i
-LIF2i
Control
CK666
SMIFH2
ARPC2 KD
20 µm
D
+LIF2i
-LIF2i
Control
CK666
SMIFH2
20 µm
E
+LIF2i
-LIF2i
pMLC
Merged
pMLC
Merged
Control
CK666
SMIFH2
20 µm

Figure 3.1. Inhibiting Arp2/3 complex but not formin activity blocks morphological changes and actin remodeling during mESC differentiation
(A) DIC images of E14 mESCs over 72h -LIF2i in the absence or presence of CK666 or SMIFH2. **(B)** Colony circularity quantified from DIC images in (A). Box plots show median, first and third quartile, with whiskers extending to observations within 1.5 times the interquartile range, and all individual data points representing means obtained from 6 independent cell preparations of 15-20 individual colonies each **(C)** Confocal images of E14 mESCs +LIF2i and -LIF2i for 72h in the absence or presence of CK666 or SMIFH2 and with Arpc2 KD labeled for F-actin with rhodamine phalloidin. **(D)** Confocal images of V6.5 mESCs +LIF2i and -LIF2i for 72h in the absence or presence of CK666 or SMIFH2 labeled for F-actin with rhodamine phalloidin. **(E)** Confocal images of E14 mESCs +LIF2i and at 72h -LIF2i in the absence or presence of CK666 or SMIFH2 and immunolabeled for pMLC (green) and stained for F-actin with rhodamine phalloidin (magenta) or nuclei with DAPI (blue). Data were analyzed by two-tailed unpaired Student's *t*-test with a significance level of $p<0.05$.

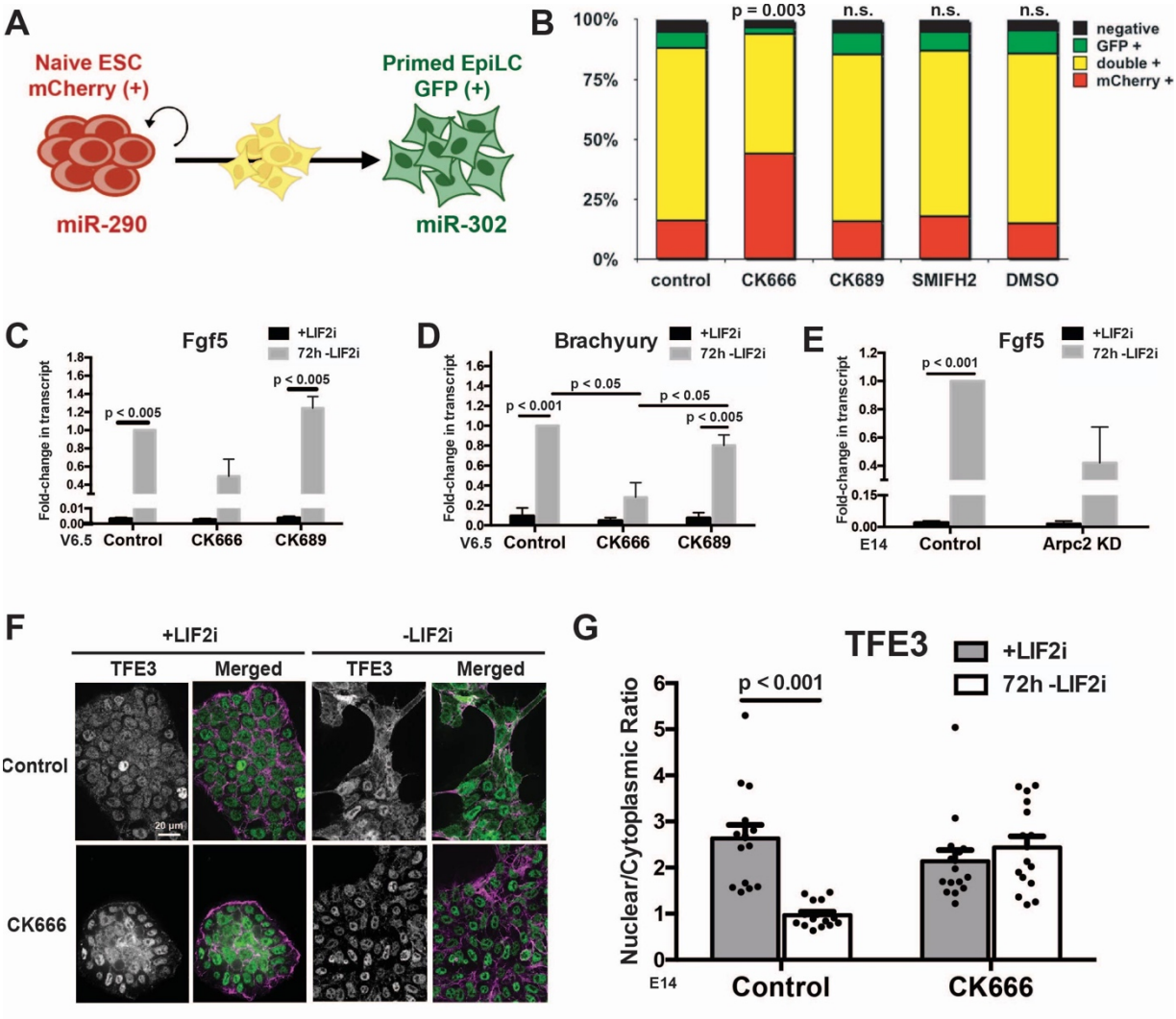

Figure 3.2. Inhibiting Arp2/3 complex but not formin activity impairs differentiation to EpiLCs

(A) Schematic of DR mESCs indicating naive self-renewing mESCs expressing *miR-290-mCherry*, primed EpiLCs expressing *miR-302-eGFP*, and cells transitioning between these stages expressing both markers. **(B)** FACS of V6.5 DR mESCs after 72h -LIF2i in the absence or presence of CK666, CK689 inactive analog of CK666, SMIFH2 or DMSO vehicle, with indicated data representing a mean from 6 independent cell preparations. **(C-E)** RT-qPCR for *Fgf5* **(C)** and *Brachyury* **(D)** in V6.5 DR mESCs and for *Fgf5* in E14 mESCs **(E)** +LIF2i and at 72h -LIF2i. Conditions include the absence (controls) or presence of CK666 or CK689 **(C,D)** and control and ARPC2 KD cells **(E)**, with data showing the means ± SEM of 3 independent cell preparations normalized to *TBP*. **(F)** Confocal images of E14 mESCs +LIF2i and at 72h -LIF2i in the absence or presence of CK666 and immunolabeled for TFE3 (green) and stained for F-actin with rhodamine phalloidin (magenta). **(G)** Quantified nuclear to cytoplasmic ratio of TFE3 immunolabeling shown in (F) indicating means ± SEM of 3 independent cell preparations. Data were analyzed by two-tailed unpaired Student's *t*-test with a significance level of $p<0.05$.

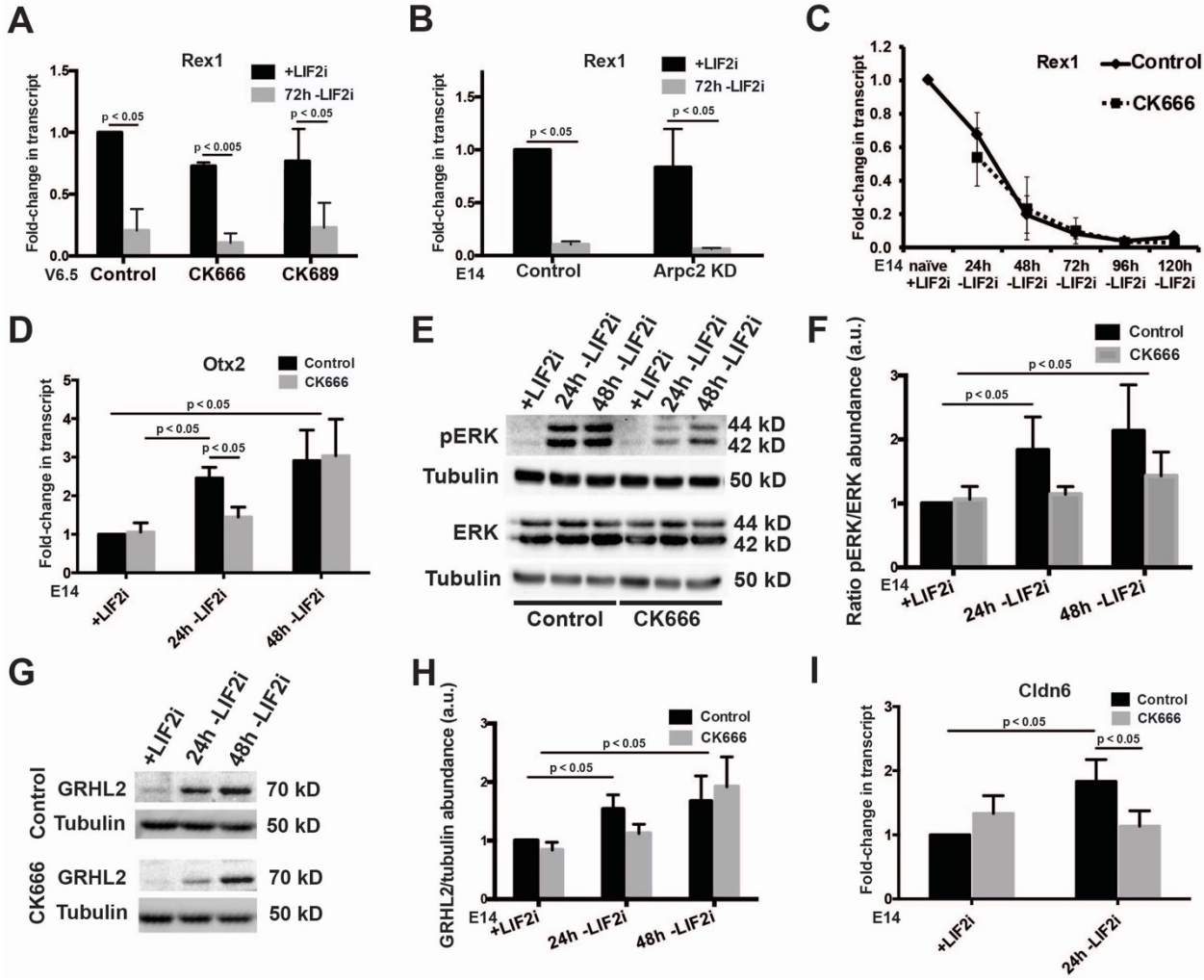

Figure 3.3. Inhibiting Arp2/3 complex activity has no effect on exit from naive self-renewal but delays entry into formative pluripotency

(A,B) RT-qPCR for *Rex1* in V6.5 DR mESCs **(A)** and E14 mESCs **(B)** +LIF2i and at 72h -LiF2i in untreated control cells and in the presence of CK666 or the inactive CK666 analog CK689 **(A)** or in ARPC2 KD cells **(B)**. Data are means ± SEM of 3 independent cell preparations normalized to *TBP*. **(C)** RT-qPCR for *Rex1* in E14 mESCs during 120h time-course -LIF2i in untreated control cells and in the presence of CK666. Data are means ± SEM of 4 independent cell preparations normalized to *TBP*. **(D)** RT-qPCR for *Otx2* in E14 mESCs during 48h time-course -LIF2i in untreated control cells and in the presence of CK666. Data are means ± SEM of 4 independent cell preparations normalized to *TBP*. **(E)** Representative immunoblot of lysates from E14 mESCs during 48h time-course -LIF2i in untreated control cells and in the presence of CK666 probed for pERK, total ERK, or tubulin as a loading control. **(F)** Semiquantitative densitometry of immunoblots described in (E), with data showing means ± SEM of 3 independent cell preparations. **(G)** Representative immunoblot of lysates from E14 mESCs during 48h time-course -LIF2i in untreated control cells and in the presence of CK666 probed for GRHL2 or tubulin as a loading control. **(H)** Semiquantitative densitometry of immunoblots described in (G), with data showing means ± SEM of 7 independent cell

preparations. **(I)** RT-qPCR for *Cldn6* in E14 mESCs after 24h -LIF2i in untreated control cells and in the presence of CK666. Data are means ± SEM of 5 independent cell preparations normalized to *TBP*. Given directional *a priori* predictions in panels D-H, data were analyzed by one-tailed unpaired Student's *t*-test with a significance level of $p<0.05$.

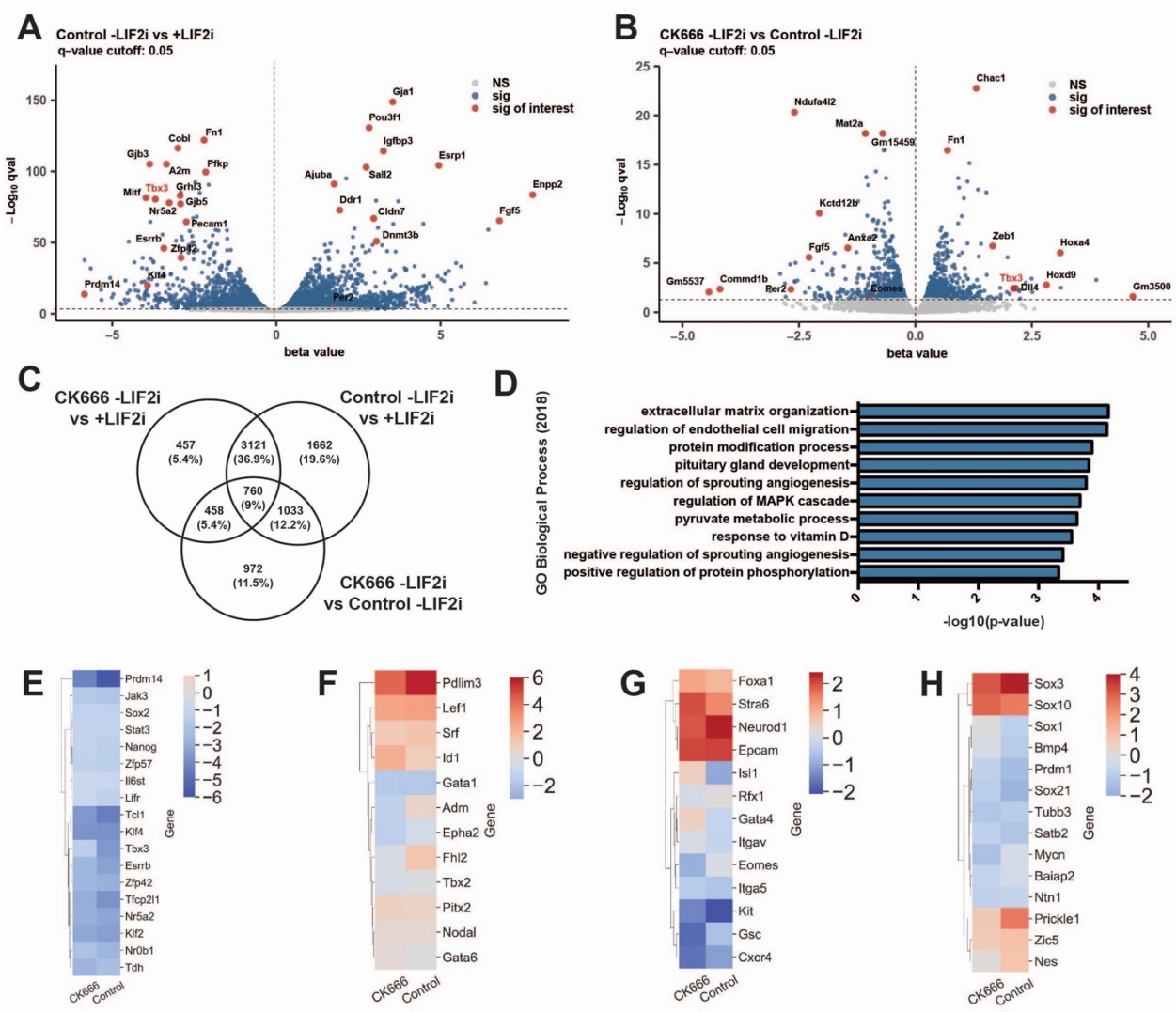

Figure 3.4. Inhibiting Arp2/3 complex activity causes global defects in lineage specification

(A) Volcano plot showing the transcriptome fold-changes (beta values) in Control -LIF2i compared with +LIF2i E14 mESCs after 72h. Each dot represents one gene with significantly changed genes (q-value<0.05) indicated in blue and significantly changed genes of interest indicated in red. **(B)** Volcano plot showing the transcriptome fold-changes (beta values) in CK666 -LIF2i compared with Control -LIF2i E14 mESCs after 72h. Each dot represents one gene with significantly changed genes (q-value<0.05) indicated in blue and significantly changed genes of interest indicated in red. **(C)** Venn diagram showing the number of shared and distinct DEGs indicated by RNA-seq for each listed comparison. **(D)** GO Biological Process (2019) enrichment analysis of 972 DEGs uniquely indicated in CK666 -LIF2i compared to Control -LIF2i after 72h. **(E-H)** Clustermap showing naive mESC marker **(E)**, mesoderm marker **(F)**, endoderm marker **(G)**, and ectoderm marker **(H)** expression indicated by beta values from RNA-seq analysis of E14 mESCs in the absence (Control) or presence of CK666 after 72h -LIF2i compared to +LIF2i.

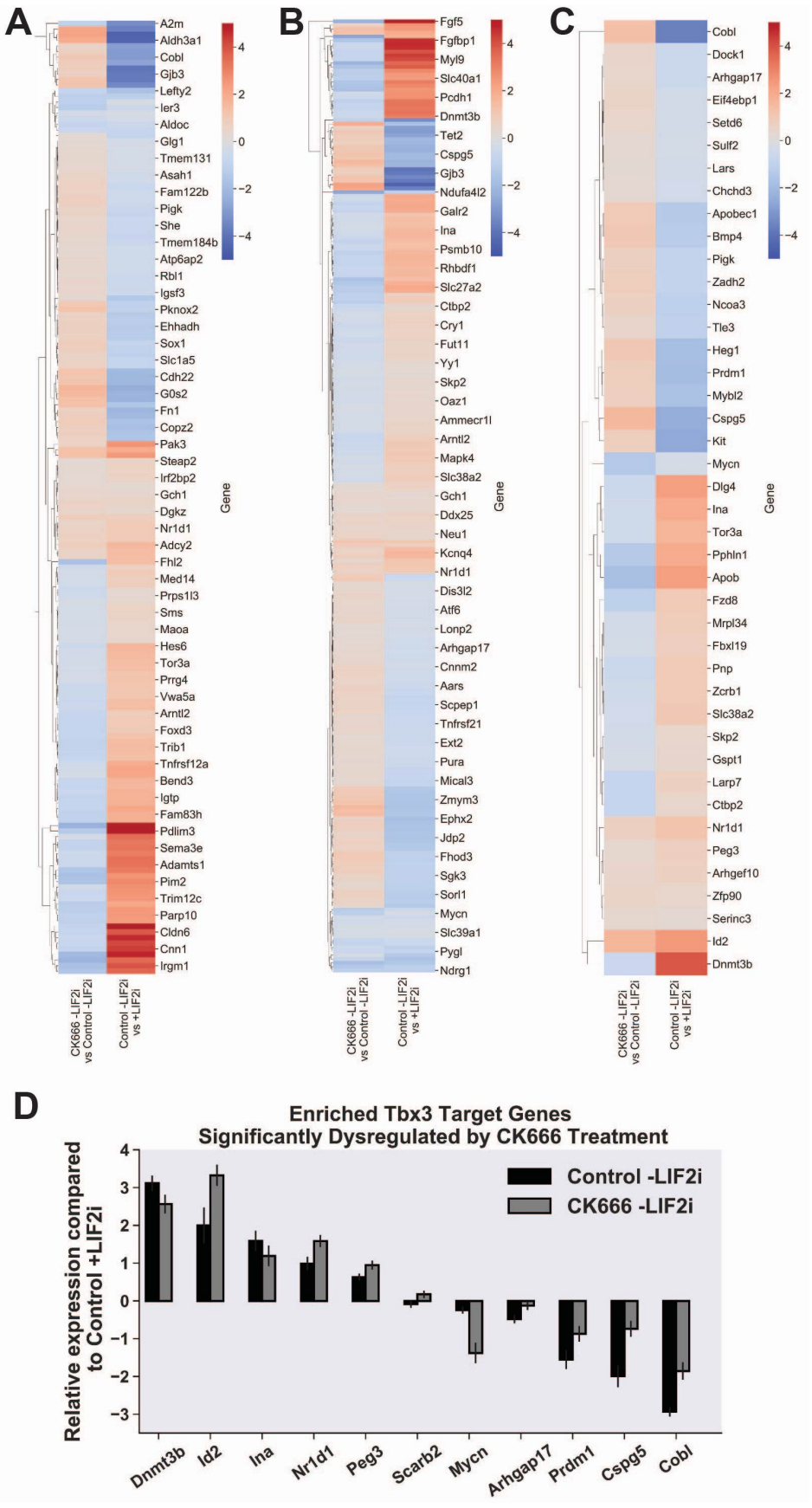
A
B
C
D
Gene
A2m
Aldh3a1
Cobl
Gjb3
Lefty2
Ier3
Aldoc
Glg1
Tmem131
Asah1
Fam122b
Pigk
She
Tmem184b
Atp6ap2
Rbl1
Igsf3
Pknox2
Ehhadh
Sox1
Slc1a5
Cdh22
G0s2
Fn1
Copz2
Pak3
Steap2
Irf2bp2
Gch1
Dgkz
Nr1d1
Adcy2
Fhl2
Med14
Prps1l3
Sms
Maoa
Hes6
Tor3a
Prrg4
Vwa5a
Arntl2
Foxd3
Trib1
Tnfrsf12a
Bend3
Igtp
Fam83h
Pdlim3
Sema3e
Adamts1
Pim2
Trim12c
Parp10
Cldn6
Cnn1
Irgm1
CK666 -LIF2i vs Control -LIF2i
Control -LIF2i vs +LIF2i
Fgf5
Fgfbp1
Myl9
Slc40a1
Pcdh1
Dnmt3b
Tet2
Cspg5
Gjb3
Ndufa4l2
Galr2
Ina
Psmb10
Rhbdf1
Slc27a2
Ctbp2
Cry1
Fut11
Yy1
Skp2
Oaz1
Ammecr1l
Arntl2
Mapk4
Slc38a2
Gch1
Ddx25
Neu1
Kcnq4
Nr1d1
Dis3l2
Atf6
Lonp2
Arhgap17
Cnnm2
Aars
Scpep1
Tnfrsf21
Ext2
Pura
Mical3
Zmym3
Ephx2
Jdp2
Fhod3
Sgk3
Sorl1
Mycn
Slc39a1
Pygl
Ndrg1
Cobl
Dock1
Arhgap17
Eif4ebp1
Setd6
Sulf2
Lars
Chchd3
Apobec1
Bmp4
Pigk
Zadh2
Ncoa3
Tle3
Heg1
Prdm1
Mybl2
Cspg5
Kit
Mycn
Dlg4
Ina
Tor3a
Pphln1
Apob
Fzd8
Mrpl34
Fbxl19
Pnp
Zcrb1
Slc38a2
Skp2
Gspt1
Larp7
Ctbp2
Nr1d1
Peg3
Arhgef10
Zfp90
Serinc3
Id2
Dnmt3b
Enriched Tbx3 Target Genes
Significantly Dysregulated by CK666 Treatment
Relative expression compared to Control +LIF2i
Control -LIF2i
CK666 -LIF2i
Dnmt3b
Id2
Ina
Nr1d1
Peg3
Scarb2
Mycn
Arhgap17
Prdm1
Cspg5
Cobl

Figure 3.5. Inhibiting Arp2/3 complex activity disrupts Tbx3-dependent transcriptional programs

(A-C) Clustermap showing expression of Tbx3 target genes identified by Russell et al., 2015 **(A),** Nishiyama et al., 2013 **(B)**, or Han et al., 2010 **(C)** with beta value fold-changes indicated from RNA-seq analysis of E14 mESCs in a control differentiation (Control -LIF2i vs +LIF2i) and how they are affected in the presence of CK666 (CK666 -LIF2i vs Control -LIF2i). **(D)** Enriched bar graph with beta value fold-changes indicated from RNA-seq analysis of E14 mESCs for commonly identified TBX3 target genes across all three published datasets (Russell et al., 2015; Nishiyama et al., 2013; Han et al., 2010) which exhibit significantly different expression (qval < 0.05) in CK666 -LIF2i compared to control -LIF2i.

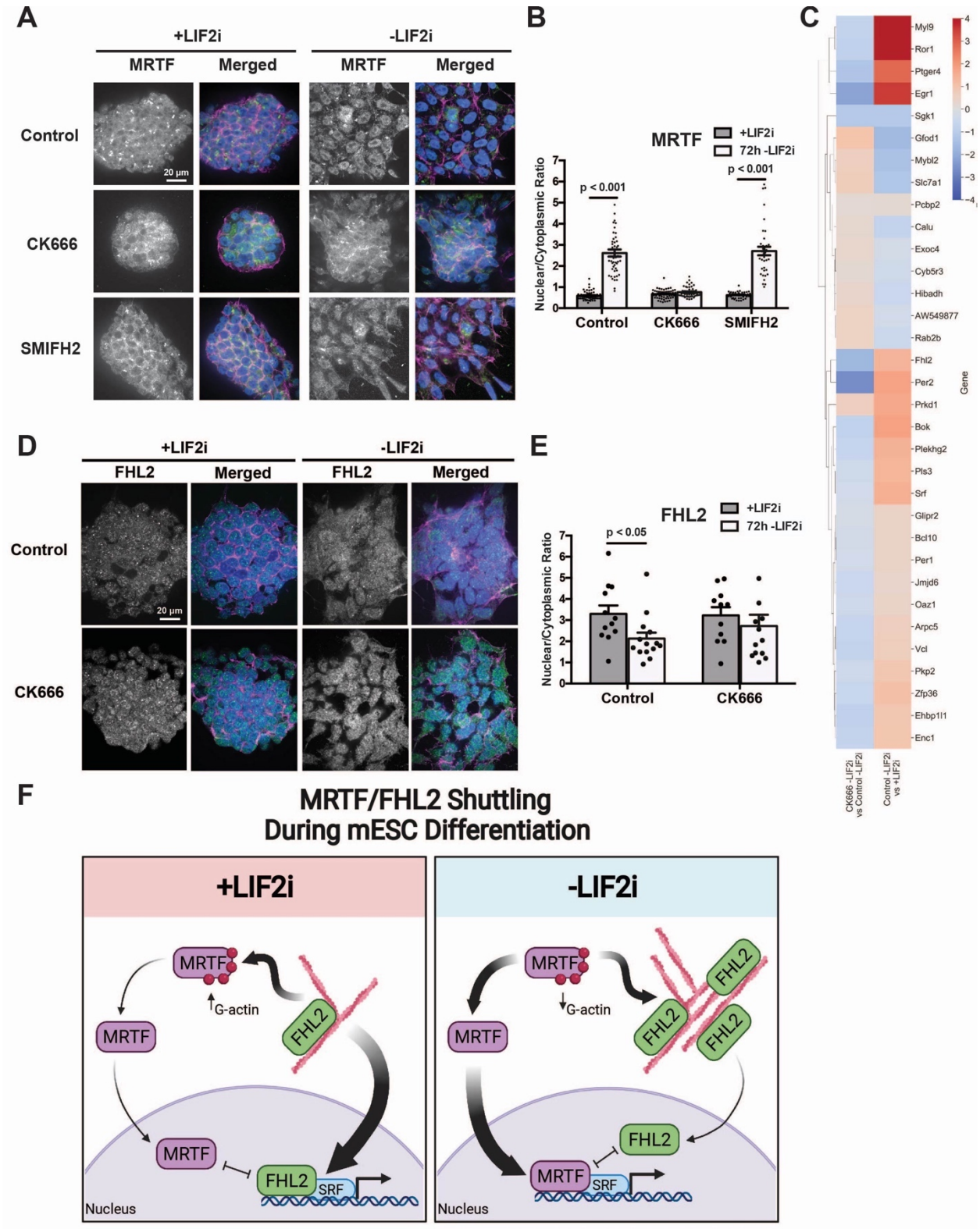
A
+LIF2i
-LIF2i
MRTF
Merged
MRTF
Merged
Control
CK666
SMIFH2
20 µm
B
MRTF
+LIF2i
72h -LIF2i
p < 0.001
p < 0.001
Nuclear/Cytoplasmic Ratio
Control
CK666
SMIFH2
C
Myl9
Ror1
Ptger4
Egr1
Sgk1
Gfod1
Mybl2
Slc7a1
Pcbp2
Calu
Exoc4
Cyb5r3
Hibadh
AW549877
Rab2b
Fhl2
Per2
Prkd1
Bok
Plekhg2
Pls3
Srf
Glipr2
Bcl10
Per1
Jmjd6
Oaz1
Arpc5
Vcl
Pkp2
Zfp36
Ehbp1l1
Enc1
Gene
CK666 -LIF2i vs Control -LIF2i
Control -LIF2i vs +LIF2i
D
+LIF2i
-LIF2i
FHL2
Merged
FHL2
Merged
Control
CK666
20 µm
E
FHL2
+LIF2i
72h -LIF2i
p < 0.05
Nuclear/Cytoplasmic Ratio
Control
CK666
F
MRTF/FHL2 Shuttling
During mESC Differentiation
+LIF2i
-LIF2i
MRTF
G-actin
FHL2
SRF
Nucleus

Figure 3.6. Inhibiting Arp2/3 complex activity blocks cytoplasmic and nuclear shuttling of FHL2 and MRTF

(A) Confocal images of E14 mESCs +LIF2i and at 72h -LIF2i in the absence or presence of CK666 or SMIFH2 immunolabeled for MRTF (green) and stained for F-actin with rhodamine phalloidin (magenta) and for nuclei with DAPI (blue). **(B)** Quantified nuclear to cytoplasmic ratio of MRTF immunolabeling shown in (A) indicating means ± SEM of 3 independent cell preparations. **(C)** Clustermap showing expression of MRTF target genes identified by Esnault et al., 2014 with beta values indicated from RNA-seq analysis of E14 mESCs in a control differentiation (Control -LIF2i vs +LIF2i) and how they are affected in the presence of CK666 (CK666 -LIF2i vs Control -LIF2i). **(D)** Confocal images of E14 mESCs +LIF2i and at 72h -LIF2i in the absence or presence of CK666 immunolabeled for FHL2 (green) and stained for F-actin with rhodamine phalloidin (magenta) and for nuclei with DAPI (blue). **(E)** Quantified nuclear to cytoplasmic ratio of FHL2 immunolabeling shown in (D) indicating means ± SEM of cells from images obtained in 4 independent cell preparations. Data were analyzed by two-tailed unpaired Student's *t*-test with a significance level of $p<0.05$. **(F)** Model of competing inverse actin-dependent MRTF/FHL2 nuclear translocation for mESCs in the presence and absence of LIF2i. Created with BioRender.com.

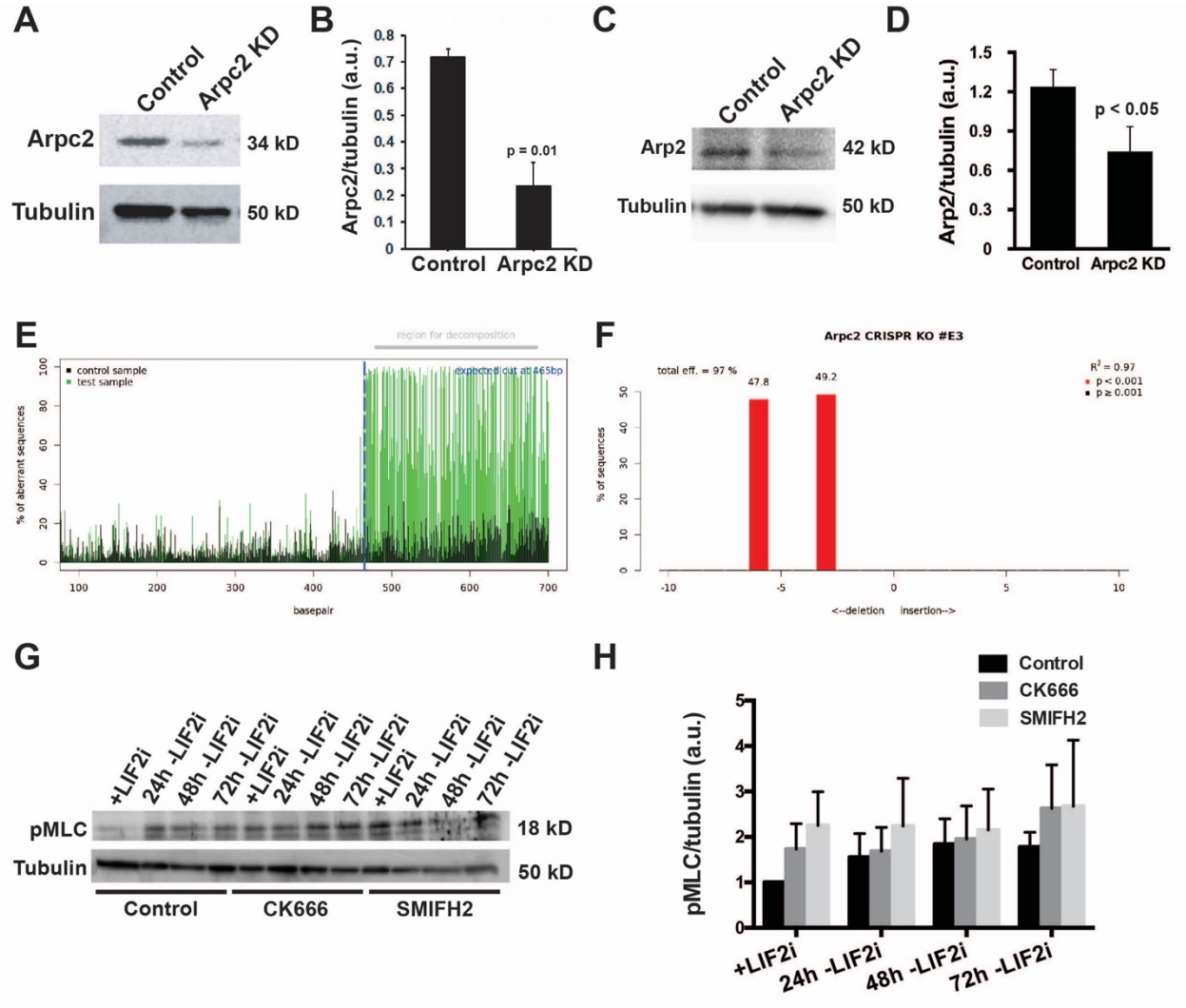

Figure 3.7. Confirming Arpc2 CRISPR KD and pMLC abundance in mESCs
(A) Representative immunoblot of lysates from E14 control or Arpc2 KD mESCs probed for ARPC2 or tubulin as a loading control. **(B)** Semiquantitative densitometry of immunoblots described in (A), with data showing means ± SEM of 3 independent cell preparations. **(C)** Representative immunoblot of lysates from E14 control or Arpc2 KD mESCs probed for ARP2 or tubulin as a loading control. **(D)** Semiquantitative densitometry of immunoblots described in (C), with data showing means ± SEM of 3 independent cell preparations. **(E)** Profile of CRISPR-Cas9 edited E14 mESCs using TIDE webtool (https://tide.deskgen.com) to quantify editing efficacy by sequence aberration compared to control cells and to **(F)** identify the predominant indel (Brinkman *et al*., Nucleic Acids Reserch 2014). **(G)** Representative immunoblot of lysates from E14 mESCs over 72h timecourse -LIF2i in the absence (control) or presence of CK666 or SMIFH2 probed for pMLC and tubulin as a loading control. **(H)** Semiquantitative densitometry of immunoblots described in (G), with data showing means ± SEM of 3 independent cell preparations. Data were analyzed by two-tailed unpaired Student's *t*-test with a significance level of $p<0.05$.

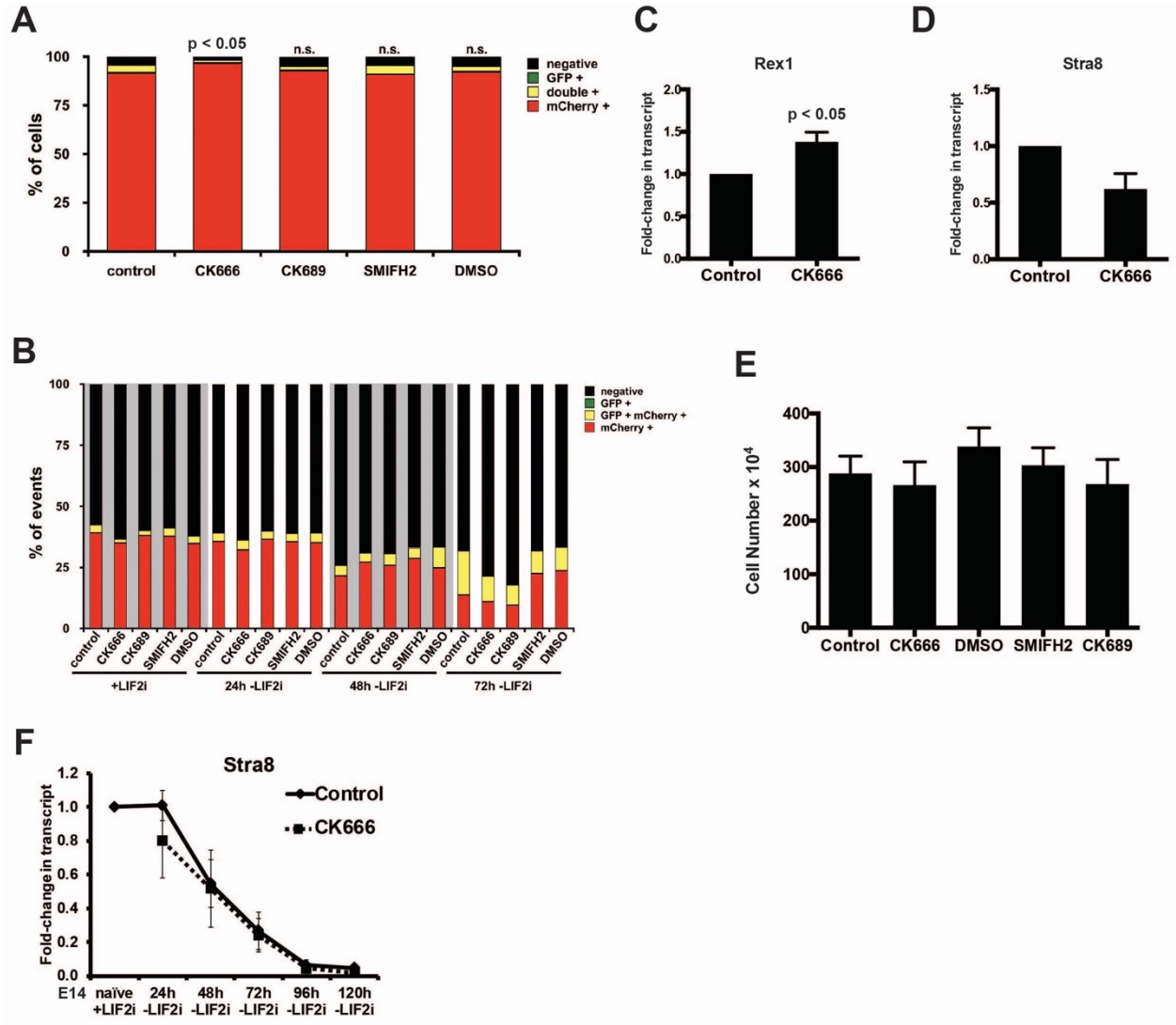

Figure 3.8. Inhibiting Arp2/3 complex activity has no effect on +LIF2i naive marker expression, cell death, or proliferation

(A) FACS of V6.5 DR mESCs at 72h with LIF2i in the absence (control) or presence of CK666, CK689 inactive analog of CK666, SMIFH2, or DMSO vehicle, with indicated data from 6 independent cell preparations. **(B)** FACS of V6. 5 DR mESCs stained with DAPI during 72h -LIF2i timecourse in the absence (control) or presence of CK666, CK689 inactive analog of CK666, SMIFH2, or DMSO vehicle, with indicated data from 6 independent cell preparations to identify the differentiation status of only dead or dying cells. **(C)** RT-qPCR for *Rex1* and **(D)** *Stra8* in E14 mESCs at 120h with LIF2i in the absence (control) or presence of CK666 with indicated data showing means ± SEM of 4 independent cell preparations normalized to *TBP*. **(E)** Number of E14 mESCs after 72h -LIF2i in the absence (control) or presence of CK666, CK689 inactive analog of CK666, SMIFH2, or DMSO vehicle, with indicated data showing means ± SEM of 3 independent cell preparations. **(F)** RT-qPCR for *Stra8* in E14 mESCs during 120h -LIF2i timecourse in the absence (control) or presence of CK666, with indicated data showing means ±

SEM of 4 independent cell preparations normalized to *TBP*. Data were analyzed by two-tailed unpaired Student's *t*-test with a significance level of $p<0.05$.

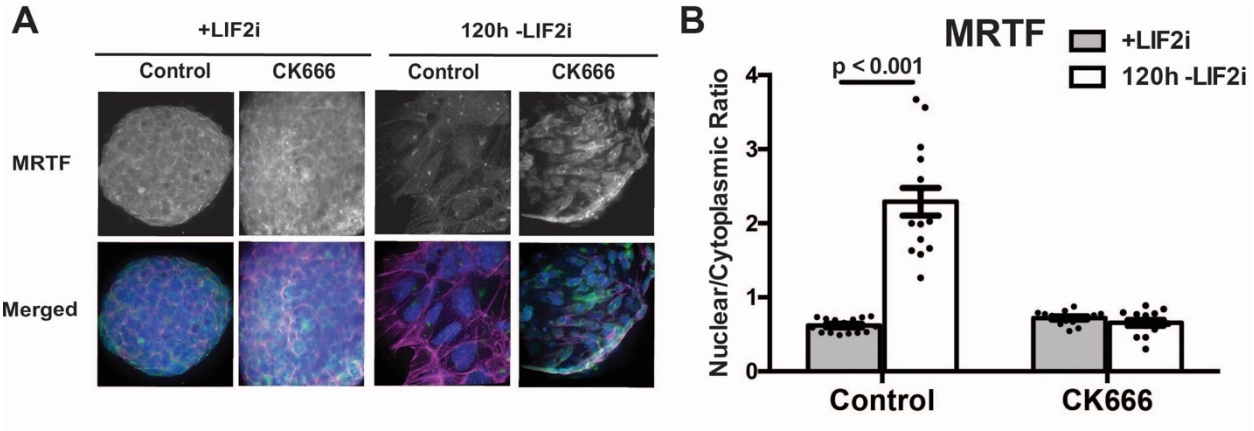

Figure 3.9. Inhibiting Arp2/3 complex activity blocks nuclear MRTF translocation at 120h -LIF2i

(A) Confocal images of E14 mESCs +LIF2i and at 120h -LIF2i in the absence or presence of CK666 immunolabeled for MRTF (green) and stained for F-actin with rhodamine phalloidin (magenta) and for nuclei with DAPI (blue). **(B)** Quantified nuclear to cytoplasmic ratio of MRTF immunolabeling shown in (A) indicating means ± SEM of 3 independent cell preparations. Data were analyzed by two-tailed unpaired Student's *t*-test with a significance level of $p<0.05$.

CHAPTER 4: ADDITIONAL PUBLICATIONS FROM THESIS RESEARCH

Formin-dependent TGF-β signaling for epithelial to mesenchymal transition

The role of distinct actin filament architectures in epithelial plasticity remains incompletely understood. We therefore determined roles for formins and the Arp2/3 complex, which are actin nucleators generating unbranched and branched actin filaments, respectively, in the process of epithelial to mesenchymal transition (EMT). In clonal lung, mammary, and renal epithelial cells, the formin activity inhibitor SMIFH2 but not the Arp2/3 complex activity inhibitor CK666 blocked EMT induced by TGF-β. SMIFH2 prevented the proximal signal of increased Smad2 phosphorylation and hence also blocked downstream EMT markers, including actin filament remodeling, decreased expression of the adherens junction protein E-cadherin, and increased expression of the matrix protein fibronectin and the transcription factor Snail. The short hairpin RNA silencing of formins DIAPH1 and DIAPH3 but not other formins phenocopied SMIFH2 effects and inhibited Smad2 phosphorylation and changes in Snail and cadherin expression. Formin activity was not necessary for the cell surface expression or dimerization of TGF-β receptors, or for nuclear translocation of TAZ, a transcription cofactor in Hippo signaling also regulated by TGF-β. Our findings reveal a previously unrecognized role for formin-dependent actin architectures in proximal TGF-β signaling that is necessary for Smad2 phosphorylation but not for cross-talk to TAZ.

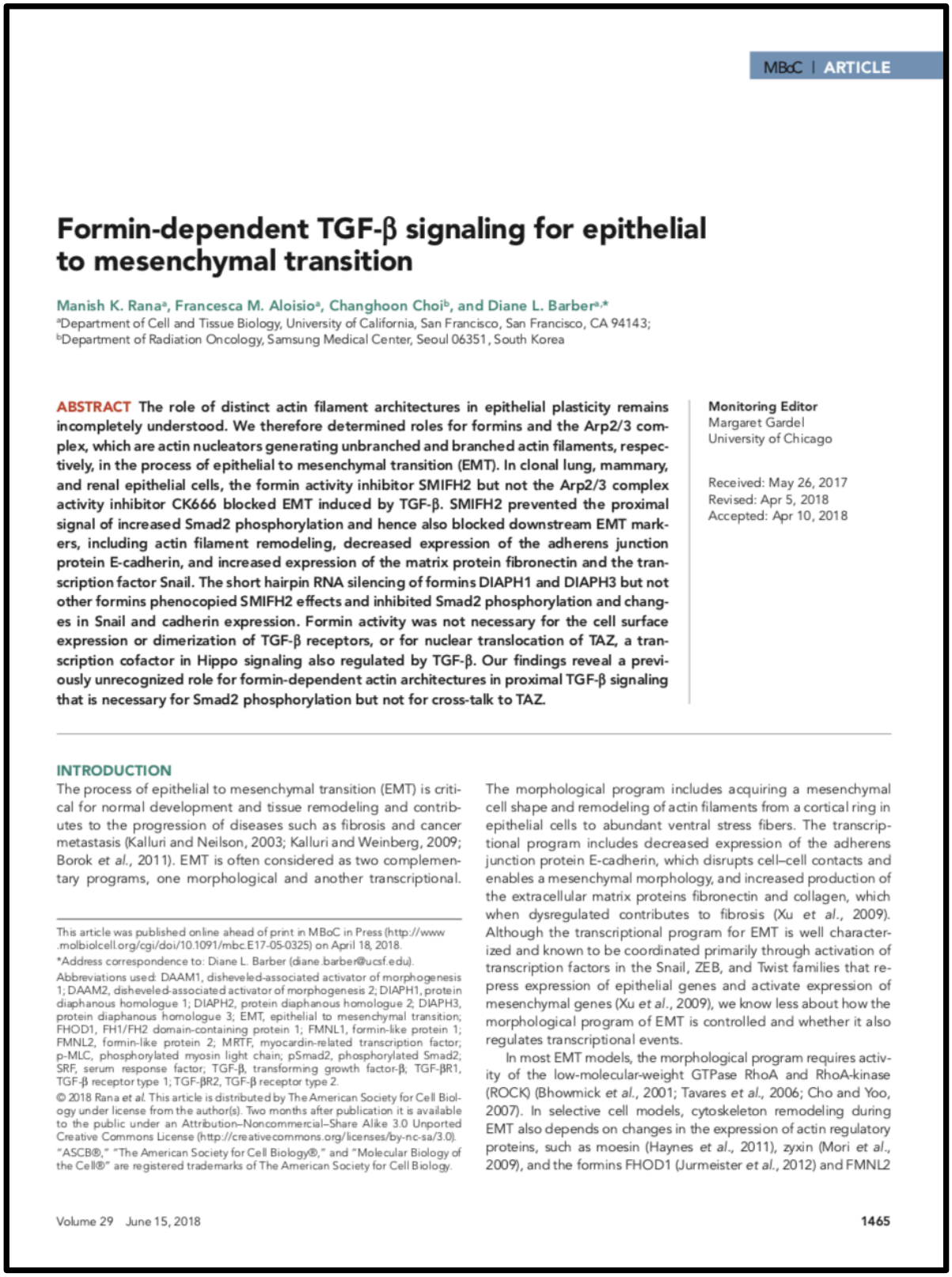

MBoC | ARTICLE

Formin-dependent TGF-β signaling for epithelial to mesenchymal transition

Manish K. Rana[a], Francesca M. Aloisio[a], Changhoon Choi[b], and Diane L. Barber[a,*]
[a]Department of Cell and Tissue Biology, University of California, San Francisco, San Francisco, CA 94143;
[b]Department of Radiation Oncology, Samsung Medical Center, Seoul 06351, South Korea

ABSTRACT The role of distinct actin filament architectures in epithelial plasticity remains incompletely understood. We therefore determined roles for formins and the Arp2/3 complex, which are actin nucleators generating unbranched and branched actin filaments, respectively, in the process of epithelial to mesenchymal transition (EMT). In clonal lung, mammary, and renal epithelial cells, the formin activity inhibitor SMIFH2 but not the Arp2/3 complex activity inhibitor CK666 blocked EMT induced by TGF-β. SMIFH2 prevented the proximal signal of increased Smad2 phosphorylation and hence also blocked downstream EMT markers, including actin filament remodeling, decreased expression of the adherens junction protein E-cadherin, and increased expression of the matrix protein fibronectin and the transcription factor Snail. The short hairpin RNA silencing of formins DIAPH1 and DIAPH3 but not other formins phenocopied SMIFH2 effects and inhibited Smad2 phosphorylation and changes in Snail and cadherin expression. Formin activity was not necessary for the cell surface expression or dimerization of TGF-β receptors, or for nuclear translocation of TAZ, a transcription cofactor in Hippo signaling also regulated by TGF-β. Our findings reveal a previously unrecognized role for formin-dependent actin architectures in proximal TGF-β signaling that is necessary for Smad2 phosphorylation but not for cross-talk to TAZ.

Monitoring Editor
Margaret Gardel
University of Chicago

Received: May 26, 2017
Revised: Apr 5, 2018
Accepted: Apr 10, 2018

INTRODUCTION

The process of epithelial to mesenchymal transition (EMT) is critical for normal development and tissue remodeling and contributes to the progression of diseases such as fibrosis and cancer metastasis (Kalluri and Neilson, 2003; Kalluri and Weinberg, 2009; Borok *et al.*, 2011). EMT is often considered as two complementary programs, one morphological and another transcriptional. The morphological program includes acquiring a mesenchymal cell shape and remodeling of actin filaments from a cortical ring in epithelial cells to abundant ventral stress fibers. The transcriptional program includes decreased expression of the adherens junction protein E-cadherin, which disrupts cell–cell contacts and enables a mesenchymal morphology, and increased production of the extracellular matrix proteins fibronectin and collagen, which when dysregulated contributes to fibrosis (Xu *et al.*, 2009). Although the transcriptional program for EMT is well characterized and known to be coordinated primarily through activation of transcription factors in the Snail, ZEB, and Twist families that repress expression of epithelial genes and activate expression of mesenchymal genes (Xu *et al.*, 2009), we know less about how the morphological program of EMT is controlled and whether it also regulates transcriptional events.

In most EMT models, the morphological program requires activity of the low-molecular-weight GTPase RhoA and RhoA-kinase (ROCK) (Bhowmick *et al.*, 2001; Tavares *et al.*, 2006; Cho and Yoo, 2007). In selective cell models, cytoskeleton remodeling during EMT also depends on changes in the expression of actin regulatory proteins, such as moesin (Haynes *et al.*, 2011), zyxin (Mori *et al.*, 2009), and the formins FHOD1 (Jurmeister *et al.*, 2012) and FMNL2

This article was published online ahead of print in MBoC in Press (http://www.molbiolcell.org/cgi/doi/10.1091/mbc.E17-05-0325) on April 18, 2018.

*Address correspondence to: Diane L. Barber (diane.barber@ucsf.edu).

Abbreviations used: DAAM1, disheveled-associated activator of morphogenesis 1; DAAM2, disheveled-associated activator of morphogenesis 2; DIAPH1, protein diaphanous homologue 1; DIAPH2, protein diaphanous homologue 2; DIAPH3, protein diaphanous homologue 3; EMT, epithelial to mesenchymal transition; FHOD1, FH1/FH2 domain-containing protein 1; FMNL1, formin-like protein 1; FMNL2, formin-like protein 2; MRTF, myocardin-related transcription factor; p-MLC, phosphorylated myosin light chain; pSmad2, phosphorylated Smad2; SRF, serum response factor; TGF-β, transforming growth factor-β; TGF-βR1, TGF-β receptor type 1; TGF-βR2, TGF-β receptor type 2.

Figure 4.1. Formin-dependent TGF-β signaling for epithelial to mesenchymal transition.

pHLARE: a new biosensor reveals decreased lysosome pH in cancer cells

Many lysosome functions are determined by a lumenal pH of ~5.0, including the activity of resident acid-activated hydrolases. Lysosome pH (pHlys) is often increased in neurodegenerative disorders and predicted to be decreased in cancers, making it a potential target for therapeutics to limit the progression of these diseases. Accurately measuring pHlys, however, is limited by currently used dyes that accumulate in multiple intracellular compartments and cannot be propagated in clonal cells for longitudinal studies or used for in vivo determinations. To resolve this limitation, we developed a genetically encoded ratiometric pHlys biosensor, pHLARE (pH Lysosomal Activity REporter), which localizes predominantly in lysosomes, has a dynamic range of pH 4.0 to 6.5, and can be stably expressed in cells. Using pHLARE we show decreased pHlys with inhibiting activity of the mammalian target of rapamycin complex 1 (mTORC1). Also, cancer cells from different tissue origins have a lower pHlys than untransformed cells, and stably expressing oncogenic RasV12 in untransformed cells is sufficient to decrease pHlys. pHLARE is a new tool to accurately measure pHlys for improved understanding of lysosome dynamics, which is increasingly considered a therapeutic target.

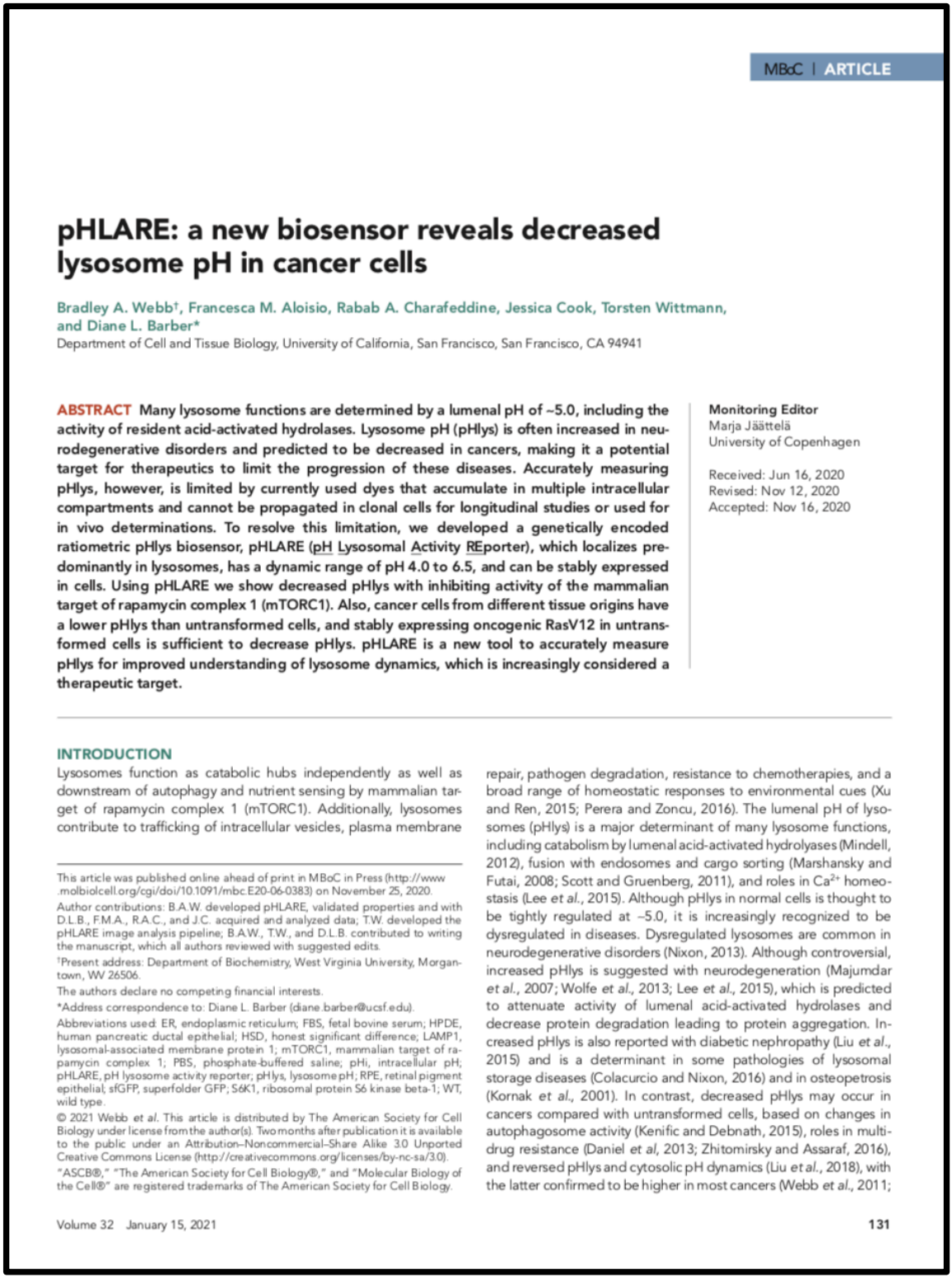

MBoC | ARTICLE

pHLARE: a new biosensor reveals decreased lysosome pH in cancer cells

Bradley A. Webb†, Francesca M. Aloisio, Rabab A. Charafeddine, Jessica Cook, Torsten Wittmann, and Diane L. Barber*
Department of Cell and Tissue Biology, University of California, San Francisco, San Francisco, CA 94941

ABSTRACT **Many lysosome functions are determined by a lumenal pH of ~5.0, including the activity of resident acid-activated hydrolases. Lysosome pH (pHlys) is often increased in neurodegenerative disorders and predicted to be decreased in cancers, making it a potential target for therapeutics to limit the progression of these diseases. Accurately measuring pHlys, however, is limited by currently used dyes that accumulate in multiple intracellular compartments and cannot be propagated in clonal cells for longitudinal studies or used for in vivo determinations. To resolve this limitation, we developed a genetically encoded ratiometric pHlys biosensor, pHLARE (pH Lysosomal Activity REporter), which localizes predominantly in lysosomes, has a dynamic range of pH 4.0 to 6.5, and can be stably expressed in cells. Using pHLARE we show decreased pHlys with inhibiting activity of the mammalian target of rapamycin complex 1 (mTORC1). Also, cancer cells from different tissue origins have a lower pHlys than untransformed cells, and stably expressing oncogenic RasV12 in untransformed cells is sufficient to decrease pHlys. pHLARE is a new tool to accurately measure pHlys for improved understanding of lysosome dynamics, which is increasingly considered a therapeutic target.**

Monitoring Editor
Marja Jäättelä
University of Copenhagen

Received: Jun 16, 2020
Revised: Nov 12, 2020
Accepted: Nov 16, 2020

INTRODUCTION

Lysosomes function as catabolic hubs independently as well as downstream of autophagy and nutrient sensing by mammalian target of rapamycin complex 1 (mTORC1). Additionally, lysosomes contribute to trafficking of intracellular vesicles, plasma membrane repair, pathogen degradation, resistance to chemotherapies, and a broad range of homeostatic responses to environmental cues (Xu and Ren, 2015; Perera and Zoncu, 2016). The lumenal pH of lysosomes (pHlys) is a major determinant of many lysosome functions, including catabolism by lumenal acid-activated hydrolyases (Mindell, 2012), fusion with endosomes and cargo sorting (Marshansky and Futai, 2008; Scott and Gruenberg, 2011), and roles in Ca^{2+} homeostasis (Lee *et al.*, 2015). Although pHlys in normal cells is thought to be tightly regulated at ~5.0, it is increasingly recognized to be dysregulated in diseases. Dysregulated lysosomes are common in neurodegenerative disorders (Nixon, 2013). Although controversial, increased pHlys is suggested with neurodegeneration (Majumdar *et al.*, 2007; Wolfe *et al.*, 2013; Lee *et al.*, 2015), which is predicted to attenuate activity of lumenal acid-activated hydrolases and decrease protein degradation leading to protein aggregation. Increased pHlys is also reported with diabetic nephropathy (Liu *et al.*, 2015) and is a determinant in some pathologies of lysosomal storage diseases (Colacurcio and Nixon, 2016) and in osteopetrosis (Kornak *et al.*, 2001). In contrast, decreased pHlys may occur in cancers compared with untransformed cells, based on changes in autophagosome activity (Kenific and Debnath, 2015), roles in multidrug resistance (Daniel *et al*, 2013; Zhitomirsky and Assaraf, 2016), and reversed pHlys and cytosolic pH dynamics (Liu *et al.*, 2018), with the latter confirmed to be higher in most cancers (Webb *et al.*, 2011;

This article was published online ahead of print in MBoC in Press (http://www.molbiolcell.org/cgi/doi/10.1091/mbc.E20-06-0383) on November 25, 2020.

Author contributions: B.A.W. developed pHLARE, validated properties and with D.L.B., F.M.A., R.A.C., and J.C. acquired and analyzed data; T.W. developed the pHLARE image analysis pipeline; B.A.W., T.W., and D.L.B. contributed to writing the manuscript, which all authors reviewed with suggested edits.

†Present address: Department of Biochemistry, West Virginia University, Morgantown, WV 26506.

The authors declare no competing financial interests.

*Address correspondence to: Diane L. Barber (diane.barber@ucsf.edu).

Abbreviations used: ER, endoplasmic reticulum; FBS, fetal bovine serum; HPDE, human pancreatic ductal epithelial; HSD, honest significant difference; LAMP1, lysosomal-associated membrane protein 1; mTORC1, mammalian target of rapamycin complex 1; PBS, phosphate-buffered saline; pHi, intracellular pH; pHLARE, pH lysosome activity reporter; pHlys, lysosome pH; RPE, retinal pigment epithelial; sfGFP, superfolder GFP; S6K1, ribosomal protein S6 kinase beta-1; WT, wild type.

Figure 4.2. pHLARE: a new biosensor reveals decreased lysosome pH in cancer cells.

CHAPTER 5: METHODS

Cell culture

Wild-type and DR V6.5 ESCs, obtained from R. Blelloch (University of California San Francisco), and E14 ESCs, provided by A. Smith (University of Cambridge) were maintained in tissue culture dishes coated with 0.2% gelatin (G1393; Sigma) at 37°C and 5% CO2 in DMEM (10569; Gibco) supplemented with 15% FBS (FB-11, Omega Scientific, Inc.), glutamine (2 mM), non-essential amino acids (0.1 mM), penicillin-streptomycin (100 U/mL Penicillium and 100 µg/mL Streptomycin), and 2-mercaptoethanol (55 µM). Cells received fresh medium every 24 h and were passaged every three days after dissociating with 0.25% Trypsin-EDTA (25200-056; Gibco). For self-renewal, cells were maintained in medium containing LIF (ESGRO Cat#ESG1106; EMD Millipore) and inhibitors for MEK (1 µM; PD0325901, Cat#S1036; Selleck Chemicals) and glycogen synthase kinase-3β (1 µM; CHIR99021, Cat#S2924; Selleck Chemicals), collectively termed LIF2i. To induce spontaneous differentiation cells were washed in PBS and then incubated in medium without LIF2i for the indicated times. CK666 (80 µM final; 182515; EMD Millipore), CK689 (80 µM final; 18217; EMD Millipore), and SMIFH2 (25 µM final; S4826; Sigma) were added at 1:000 from stock solutions prepared in DMSO at the indicated times and included in medium replacements every 24h.

CRISPR/Cas9 gene editing

The validated guide RNAs (gRNA) targeting the Arpc2 locus were selected from the Genome-scale CRISPR Knock-Out (GeCKO) v2 mouse library (www.genome-engineering.org) (Sanjana et al., 2014). After annealing and adding BbsI cut site

overhangs, candidate gRNAs were cloned into the pSpCas9(BB)-2A-GFP (PX458) plasmid vector (Addgene plasmid #48138; RRID: Addgene_48138) (Ran et al., 2013). At 48 h after transfecting cells with plasmids, single GFP(+) cells were sorted by fluorescence-activated cell sorting as described below. Edited clones were validated by PCR and sequencing (forward primer AGCTGTTGAATGCAATGAGG, reverse primer TCCTCTGGGTAAAGGACCT) and confirmed by immunoblotting as described below. TIDE webtool (https://tide.deskgen.com) was used to quantify editing efficacy and identify the predominant type of indel in the edited clone (Brinkman et al., 2014). The sgRNA sequence used to generate the confirmed Arpc2 edited clone was as follows: TTCTTGGTAAATCCAGAACC.

DIC image acquisition and quantitative analysis

For DIC imaging, naïve E14 ESCs were plated for 24h on gelatin-coated glass bottom microwell dishes (P35G-1.5-14-C; MatTek) in medium containing LIF2i, washed with PBS, and then maintained for the indicated times in medium without LIF2i. CK666 and SMIFH2, as indicated above, were added at the time of LIF2i removal and replaced every 24h until completion of imaging. Live cells were imaged using a Plan Apo 40 0.95 NA objective on an inverted spinning disc microscope system (Nikon Eclipse TE2000 Perfect Focus System; Nikon Instruments; Nikon Instruments) equipped with D-C DIC Slider 40x I (MBH76240; Technical Instruments), a multipoint stage (MS-2000; Applied Scientific Instruments), a CoolSnap HQ2 cooled charge-coupled camera (Photometrics) and camera-triggered electronic shutters controlled with NIS-Elements Imaging Software (Nikon). Approximately 15-20 colonies were imaged for each condition and time point.

Colony circularity was quantified using the ImageJ plug-in “Circularity” feature. In brief, this feature is an extended version of the Measure command in ImageJ that calculates object circularity using the formula *circularity = 4pi(area/perimeter^2)*, with a circularity value of 1.0 indicating a perfect circle. As the value approaches 0.0, it indicates an increasingly elongated polygon. Statistical analysis was performed with GraphPad Prism 6 software.

Immunolabeling, staining, and image acquisition

For immunolabeling, cells were plated on gelatin-coated coverslips prepared in an ultrasonic cleaning bath. In brief, coverslips were sonicated for 20 minutes in the presence of ddH2O and Versa detergent, washed in ddH2O, sonicated again for 20 minutes, and stored in 70% EtOH. Cells were maintained for the indicated times, washed with PBS, and fixed with 4% formaldehyde for 15 min at RT. Cells were then permeabilized with 0.1% Triton X-100 for 5 min, incubated with blocking buffer of 5% horse serum and 1% BSA in PBS for 1h, and then incubated with primary antibodies overnight at 4°C. The cells were then washed with PBS, incubated for 1h at RT with secondary antibodies conjugated with fluorophores, and washed with PBS. One wash included Hoechst 33342 (1:10,000; H-3570; Molecular Probes) to stain nuclei. Primary antibodies included Phospho-Myosin Light Chain 2 Thr18/Ser19 E2J8F (1:200; #95777; Cell Signaling Technology), MRTF-A-C19 (1:200; sc-21558; Santa Cruz Biotechnologies), FHL2 (1:200; HPA006028; Sigma), and TFE3 (1:200; 14480-1-AP; Proteintech). Actin filaments were labeled with rhodamine-phalloidin (1:400; Invitrogen) added during secondary antibody incubations. Cells were imaged using a 60X Plan Apochromat TIRF 1.45 NA oil immersion objective

on an inverted microscope system (Nikon Eclipse TE2000 Perfect Focus System; Nikon Instruments) equipped with a spinning-disk confocal scanner unit (CSU10; Yokogawa), a 488-nm solid-state laser (LMM5; Spectral Applied Research), a multipoint stage (MS-2000; Applied Scientific Instruments), a CoolSnap HQ2 cooled charge-coupled camera (Photometrics) and camera-triggered electronic shutters controlled with NIS-Elements Imaging Software (Nikon). Nuclear-to-cytoplasmic ratios were quantified using NIS-Elements Imaging Software (Nikon). Briefly, the fluorescence in the nucleus and cytoplasm were manually sampled by selection of regions-of-interest either colocalized with nuclear DAPI or not. The ratio of fluorescence was then calculated by dividing the nuclear fluorescence intensity with that of the cytoplasm for a given cell. Statistical analysis was performed in Excel (Microsoft) using two-tailed t-test.

Flow Cytometry

DR ESCs and CRISPR-Cas9 edited E14 ESCs were prepared for flow cytometry by washing with PBS at the indicated times, dissociated with 0.25% Trypsin-EDTA, and collected by centrifuging at 1000 rpm for 3 min at room temperature. Pelleted cells were washed in cold PBS, pelleted again by centrifugation, and then resuspended to a final concentration of 5-10 $x10^6$ cells/ml in PBS supplemented with 1% BSA. Cell suspensions were filtered into round-bottomed tubes with cell-strainer caps (352235; Falcon). DR ESCs were sorted using an LSR II flow cytometer (BD Biosciences) and CRISPR-Cas9 edited E14 ESCs were sorted using FACSAria III flow cytometer (BD Biosciences), and analysis was performed using FACSDiva software (BD Biosciences). Statistical analysis was performed in Excel (Microsoft) using two-tailed t-test.

RNA extraction, cDNA synthesis, and qPCR

Total RNA was isolated from ESCs at the indicated times by using TRIzol Reagent (15596026; Ambion) according to the manufacturer's protocol with the following modifications: after washing cells with PBS 800 µl TRIzol was added to cells in a six-well plate and the pellet was rinsed in 75% EtOH. RNA purity was assessed on a Nanodrop spectrometer. cDNA was synthesized using the iScript cDNA Synthesis Kit according to manufacturer's protocol (170-8891; Bio-Rad Laboratories). Quantitative PCR was performed with iQ SYBR® Green Supermix (170-8880; Bio-Rad Laboratories) according to the manufacturer's protocol on a QuantStudio 6 Flex Real-Time PCR System (Applied Biosystems), with data analyzed using GraphPad Prism 6 software. For the stem cell lineage plate array, RNA was collected using TRIzol as indicated above. cDNA was synthesized using the RT2 First Strand Synthesis Kit according to manufacturer's protocol (33041; Qiagen).

Immunoblotting

Cells were lysed for 10 min in RIPA buffer (2.5 mM HEPES pH 7.5, 150 mM NaCl, 3mM KCl, 1% NP-40, 0.5% deoxycholate, 0.1% SDS, 1 mM vanadate, and 5 mM NaF supplemented with protease and phosphatase inhibitors). Lysates were centrifuged at 13,000 rpm for 15 min to obtain a post-nuclear supernatant. Proteins were separated by SDS-PAGE and transferred onto Immobilon-P® PVDF transfer membranes (IPVH00010; EMD Millipore) as previously described (Haynes et al., 2011; Rana et al., 2015). Membranes were blocked with 5% non-fat milk in TBS containing 0.1% Tween (TBST)

and incubated with primary antibodies overnight at 4°C. Primary antibodies included α-tubulin (1:2000; GT114; GeneTex), Phospho-Myosin Light Chain 2 Thr18/Ser19 E2J8F (1:1000; #95777; Cell Signaling Technology), ERK 1 C-16 (1:1000; sc-93; Santa Cruz Biotechnology, Inc.), Phospho-p44/42 MAPK Erk1/2 Thr202/Tyr204 (1:1000; #9101; Cell Signaling Technology), Grhl2 (1:1000; HPA004820; Sigma), Arp2 (1:1000; A6104; Sigma), and Arpc2 (1:1000; 07-227; EMD Millipore). After washing, membranes were incubated in TBST with 5% non-fat milk and horseradish peroxidase (HRP)-conjugated secondary antibodies (1:10,000; 170-6516 and 172-1019; Bio Rad Laboratories) for 1 h at room temperature. After washing, immunoreactivity was developed with enhanced femto chemiluminescence (1859022 and 1859023; Thermo Scientific) and imaged using a BioRad Chemidoc XRS. ImageJ software was used for semi-quantitative densitometry analysis. Data presentation and statistical analysis were preformed using Excel Analyze-it and GraphPad Prism 6 software.

Library preparation and RNA sequencing

RNA was extracted with the RNeasy Mini kit (Qiagen, 74104) according to the manufacturer's instructions and sample concentrations were determined by NanoDrop. RNA degradation and contamination were monitored on 1% agarose gels, RNA purity was checked using the NanoPhotometer spectrophotometer (IMPLEN, CA, USA), and RNA integrity and quantitation were assessed using the RNA Nano 6000 Assay Kit of the Bioanalyzer 2100 system (Agilent Technologies, CA, USA). A total of 9 RNA libraries were prepared with three paired biological replicates for each condition including control +LIF2i, control 72h -LIF2i, and CK666 72h -LIF2i. A total amount of 1 μg RNA per sample

was used as input material for the RNA sample preparations. Sequencing libraries were generated using NEBNext Ultra RNA Library Prep Kit for Illumina (NEB, USA) following manufacturer's recommendations and index codes were added to attribute sequences to each sample. Briefly, mRNA was purified from total RNA using poly-T oligo-attached magnetic beads. Fragmentation was carried out using divalent cations under elevated temperature in NEBNext First Strand Synthesis Reaction Buffer (5X). First strand cDNA was synthesized using random hexamer primer and M-MuLV Reverse Transcriptase (RNase H). Second strand cDNA synthesis was subsequently performed using DNA Polymerase I and RNase H. Remaining overhangs were converted into blunt ends via exonuclease/polymerase activities. After adenylation of 3' ends of DNA fragments, NEBNext Adaptor with hairpin loop structure was ligated to prepare for hybridization. To select cDNA fragments of preferentially 150~200 bp in length, the library fragments were purified with AMPure XP system (Beckman Coulter, Beverly, USA). Then 3 μl USER Enzyme (NEB, USA) was used with size-selected, adaptor- ligated cDNA at 37°C for 15 min followed by 5 min at 95°C before PCR. Then PCR was performed with Phusion High-Fidelity DNA polymerase, Universal PCR primers and Index (X) Primer. At last, PCR products were purified (AMPure XP system) and library quality was assessed on the Agilent Bioanalyzer 2100 system. The clustering of the index-coded samples was performed on a cBot Cluster Generation System using PE Cluster Kit cBot-HS (Illumina) according to the manufacturer's instructions. After cluster generation, the library preparations were sequenced on an Illumina platform and paired-end reads were generated with >20 million reads per sample. The above protocol, with the exception of RNA extraction, was performed externally by Novogene Co. Ltd (USA).

RNA sequencing analysis

Quality assessment and basic processing of the reads was performed using the FastQC program (http://www.bioinformatics.babraham.ac.uk/projects/fastqc). Sequencing adapters were trimmed from the 3′ ends of the reads using cutadapt (v.1.8.1; https://pypi.python.org/pypi/cutadapt/1.8.1). We quantified transcript abundance with Kallisto (Bray et al., 2016) and built index with reference to the GRCh38 reference transcriptome. Expression analysis was performed using Sleuth (Pimentel et al., 2017) to assess differentially expressed genes between +LIF2i, control -LIF2i, and CK666 -LIF2i. Differentially expressed genes were identified using the Wald test with a cut-off of qval <0.05. Gene ontology enrichment analysis performed using Enrichr (Chen et al., 2013; Kuleshov et al., 2016). Heatmap figures were generated with Python using pandas dataframe (McKinney, 2010) input to the seaborn library (Waskom, 2021) in matplotlib (Hunter, 2007).

Dataset acquisition

CHIP-seq data of TBX3 binding in mESCs was available from NCBI (GEO Series accession number: GSE19219) (Han et al., 2010). Microarray data from shRNA TBX3 knockdown mESCs was available from NCBI (GEO Series accession number: GSE26520) (Nishiyama et al., 2013). RNA-seq data from TBX3-HI and TBX3-LO mESCs was available from NCBI (GEO Series accession number: GSE73862) (Russell et al., 2015). CHIP-seq data of MRTF binding in NIH3T3 fibroblasts was available from NCBI (GEO Series accession number: GSE45888) (Esnault et al., 2014).

Data and Code Availability

RNA-sequencing data generated during this study have been deposited in Gene Expression Omnibus (https://www.ncbi.nlm.nih.gov/geo/) under Accession code GEO: GSE175391. Software/packages used to analyze the dataset are freely available.

Tables

Table 5.1. List of primers

qPCR Primer Name	Sequence
Otx2_Forward	AATCAACTTGCCAGAATCCAGGG
Otx2_Reverse	GCTGTTGGCGGCACTTAGC
Rex1_Forward	CTCCTGCACACAGAAGAAAGC
Rex1_Reverse	CACTGATCCGCAAACACC
Stra8_Forward	GTTTCCTGCGTGTTCCACAAG
Stra8_Reverse	CACCCGAGGCTCAAGCTTC
Fgf5_Forward	CCTTGCGACCCAGGAGCTTA
Fgf5_Reverse	CCGTCTGTGGTTTCTGTTGAGG
Brachyury_Forward	CTGGGAGCTCAGTTCTTTCGA
Brachyury_Reverse	GAGGACGTGGCAGCTGAGA
Sox17_Forward	CGAGCCAAAGCGGAGTCTC
Sox17_Reverse	TGCCAAGGTCAACGCCTTC
Gsc_Forward	CAGATGCTGCCCTACATGAAC
Gsc_Reverse	TCTGGGTACTTCGTCTCCTGG
Foxa2_Forward	GTCGTCCGAGCAGCAACATC
Foxa2_Reverse	GGGTAGTGCATGACCTGTTCGTAG
Flk1_Forward	GGGATGGTCCTTGCATCAGAA
Flk1_Reverse	ACTGGTAGCCACTGGTCTGGTTG
CD34_Forward	AAGGCTGGGTGAAGACCCTTA
CD34_Reverse	TGAATGGCCGTTTCTGGAAGT
Bglap_Forward	GGACCATCTTTCTGCTCACTC
Bglap_Reverse	CCGCTGGGCTTGGCATCTG
MyoD1_Forward	CCACTCCGGGACATAGACTTG
MyoD1_Reverse	AAAAGCGCAGGTCTGGTGAG
Nestin_Forward	CCCTGAAGTCGAGGAGCTG
Nestin_Reverse	CTGCTGCACCTCTAAGCGA
Zic1_Forward	AAACTGGTCAACCACATCCG
Zic1_Reverse	AACTCGCACTTGAAGG
Krt14_Forward	AAGGTCATGGATGTGCACGAT
Krt14_Reverse	CAGCATGTAGCAGCTTTAGTTCTTG
Cldn6_Forward	AGACAAAGCTGACCGAGCAC
Cldn6_Reverse	GTTGACCCAGCCAAGCAG
TBP_Forward	GAAGAACAATCCAGACTAGCAGCA
TBP_Reverse	CCTTATAGGGAACTTCACATCACAG

Table 5.2. List of antibodies

Antibody Name	Vendor	Cat#	Notes
α-tubulin	GeneTex	GT114	1:2000 IB
Arpc2	EMD Millipore	07-227	1:1000 IB
Arp2	Sigma	A6104	1:1000 IB
ERK 1 C-16	Santa Cruz Biotechnologies	sc-93	1:1000 IB
Phospho-p44/42 MAPK Erk1/2 Thr202/Tyr204	Cell Signaling Technology	9101	1:1000 IB
FHL2	Sigma	HPA006028	1:200 IF
GRHL2	Sigma	HPA004820	1:1000 IB
MRTF-A-C19	Santa Cruz Biotechnologies	sc-21558	1:200 IF
Phospho-Myosin Light Chain 2 Thr18/Ser19 E2J8F	Cell Signaling Technology	95777	1:200 IF, 1:1000 IB
TFE3	Proteintech	14480-1-AP	1:200 IF

CHAPTER 6: CONCLUDING REMARKS

Summary

Understanding the cell biology of embryonic stem cell differentiation and fate specification is essential for a more complete understanding of developmental biology and for advancing approaches in regenerative medicine. For decades, researchers have studied transcriptional and epigenetic control of mESC differentiation but the significance of morphological changes and their role in transcriptional programs during lineage specification remain less defined. We show that Arp2/3 complex activity is necessary for differentiation of mESCs. We report that changes in colony morphology and actin architecture occur with differentiation that are dependent on Arp2/3 complex but not formin activity. Our data also indicate that Arp2/3 complex activity is necessary for pluripotent state transition: while inhibiting Arp2/3 complex activity pharmacologically or genetically has no effect on exit from naive self-renewal, loss of Arp2/3 complex activity delays entry into the formative pluripotent state, a recently identified intermediate state when cells are most competent for lineage specification. Further, we include a global examination of Arp2/3 complex activity-dependent lineage specification across all three germ layers with marked effects on TBX3-dependent transcriptional programs using RNA-sequencing. Lastly, we identify two previously unreported markers of mESC differentiation – the reciprocal nuclear translocation of competing SRF co-factors MRTF and FHL2, which is dependent upon Arp2/3 complex activity. Together, these data reveal a previously unrecognized role for the Arp2/3 complex in mESC differentiation, opening new directions for how actin remodeling broadly facilitates lineage specification during entry to formative pluripotency for insights relevant to development and regenerative medicine.

Future Directions

Distinct actin architectures with different properties drive myriad cell processes. Findings during my thesis research indicate that Arp2/3 complex but not formin activity is necessary for mESC differentiation. In contrast, we found that formin but not Arp2/3 complex activity is necessary for TGFβ-induced EMT (Rana et al., 2018). Both programs initiate from similar compact cuboidal epithelial cells with a cortical ring of unbranched actin filaments. Also, both programs result in differentiated cells with similar morphologies of elongated cell shapes but with distinct actin architectures. Taken together, these findings indicate distinct actin nucleators regulating distinct modes of epithelial plasticity, which highlight two important questions for future study. First, *how does Arp2/3 complex regulation of transcription interface within the context of other existing programs of actin-related transcriptional programs? Second, how are they similar or different? How can they inform our understanding of form and function in epithelial plasticity?*

Nuclear translocation of the SRF transcriptional co-activator MRTF has been shown during adult mesenchymal stem cell differentiation where it responds to cell spreading on a stiff substrate to promote osteogenic gene programs. My findings show that MRTF translocation occurs during naive to primed mESC differentiation and is dependent on Arp2/3 complex activity but not formin activity. Further, my RNA sequencing data show attenuated transcriptional effects on MRTF target genes in mESCs differentiated in the presence of Arp2/3 complex inhibitor CK666, suggesting a functional outcome to blocking nuclear translocation of MRTF in mESCs. Hence, an important question to resolve is *whether MRTF translocation is necessary and/or sufficient for mESC*

differentiation. This question could be addressed by asking whether expressing a constitutively nuclear-localized MRTF mutant in mESCs rescues differentiation in the presence of CK666? Also, one could test the prediction that expressing a cytosolic MRTF mutant would phenocopy impaired differentiation in the absence of CK666.

Arp2/3 complex activity is regulated by multiple upstream activators that are components of diverse signaling networks, which in turn respond to different chemical and mechanical cues. Binding to nucleation promoting factors (NPFs) such as N-WASP and WAVE are critical to activate the Arp2/3 complex. However, recent findings from the Barber lab indicate that Arp2/3 complex is a coincidence detector that requires phosphorylation of the Arp2 subunit as well as NPF binding for increased activity. Hence, an important next step is to identify which NPF and which kinase mediate Arp2/3 complex activity during mESC differentiation. *Which NPF and kinase are activating the Arp2/3 complex during entry into formative pluripotency? Which pathways are the indicated NPF and kinase responding to and how might we manipulate them to promote formative pluripotent lineage specification and enhance protocols for directed differentiation?*

REFERENCES

Azami, T., Bassalert, C., Allègre, N., Estrella, L.V., Pouchin, P., Ema, M., and Chazaud, C. (2019). Regulation of the ERK signalling pathway in the developing mouse blastocyst. Development *146(14)*, dev177139.

Baarlink, C., Wang, H., and Grosse, R. (2013). Nuclear actin network assembly by formins regulates the SRF coactivator MAL. Science *340(6134)*, 864-867.

Bailly, M., Ichetovin, I., Grant, W., Zebda, N., Machesky, L.M., Segall, J.E., and Condeelis, J. (2001). The F-actin side binding activity of the Arp2/3 complex is essential for actin nucleation and lamellipod extension. Curr Biol *11(8),* 620-625.

Bedzhov, I., Alotaibi, H., Basilicata, M.F., Ahlborn, K., Liszewska, E., Brabletz, T., and Stemmler, M.P. (2013). Adhesion, but not a specific cadherin code, is indispensable for ES cell and induced pluripotency. Stem Cell Res *11*, 1250-1263.

Belin, B.J., and Mullins, R.D. (2013). What we talk about when we talk about nuclear actin. Nucleus *4(4)*, 291-297.

Bergert, M., Lembo, S., Sharma, S., Russo, L., Milovanović, D., Gretarsson, K.H., Börmel, M., Neveu, P.A., Hackett, J.A., Petsalaki, E., and Diz-Muñoz, A. (2021). Cell surfact mechanics gate embryonic stem cell differentiation. Cell Stem Cell *28*, 209-216.

Betschinger, J., Nichols, J., Dietmann, S., Corrin, P.D., Paddison, P.J., and Smith, A. (2013). Exit from pluripotency is gated by intracellular redistribution of the bHLH transcription factor Tfe3. Cell *153(2)*, 335-347.

Bian, H., Lin, J.Z., Li, C., and Farmer, S.R. (2016). Myocardin-related transcription factor A (MRTFA) regulates the fate of bone marrow mesenchymal stem cells and its absence in mice leads to osteopenia. Mol Metab *5*, 970-979.

Bongiorno, T., Gura, J., Talwar, P., Chambers, D., Young, K.M., Arafat, D., Wang, G., Jackson-Holmes, E.L., Qiu, P., McDevitt., T.C., and Sulchek, T. (2018). Biophysical subsets of embryonic stem cells display distinct phenotypic and morphological signatures. PLOS ONE *13(3)*, e0192631.

Bray, N.L., Pimental, H., Melsted, P., and Pachter, L. (2016). Near-optimal probabilistic RNA-seq quantification. Nat Biotechnol *34*, 525-527.

Brinkman, E.K., Chen, T., Amendola, M., and van Steensel, B. (2014). Easy quantitative assessment of genome editing by sequence trace decomposition. Nucleic Acids Res *42(22)*, e168.

Brizzi, M.F., Tarone, G., and Defilippi, P. (2012). Extracellular matrix, integrins, and growth factors as tailors of the stem cell niche. Curr Opin Cell Biol *24*, 645-651.

Burianek, L.E., and Soderling, S.H. (2013). Under lock and key: spatiotemporal regulation of WASP family proteins coordinates separate dynamic cellular processes. Semin Cell Dev Biol *24(4)*, 258-266.

Carlson, H., Ota, S., Campbell, C.E., and Hurlin, P.J. (2001). A dominant repression domain in Tbx3 mediates transcriptional repression and cell immortalization: relevance to mutations in Tbx3 that cause ulnar-mammary syndrome. Hum Mol Genet *10(21)*, 2403-2413.

Carroll, E.A., Gerrelli, D., Gasca, S., Berg, E., Beier, D.R., Copp, A.J., and Klingensmith, J. (2003). Cordon-bleu is a conserved gene involved in neural tube formation. Dev Biol *262(1)*, 16-31.

Chhabra, E.S., and Higgs, H.N. (2007). The many faces of actin: matching assembly factors with cellular structures. Nat Cell Biol *9*, 1110-1121.

Chapman, D.L., Garvey, N., Hancock, S., Alexiou, M., Agulnik, S.I., Gibson-Brown, J.J., Cebra-Thomas, J., Bollag, R.J., Silver, L.M., and Papaioannou, V.E. (1996). Expression of the T-box family genes, Tbx1-Tbx5, during early mouse development. Dev Dyn *206(4)*, 379-390.

Charras, G., and Yap, A.S. (2018). Tensile Forces and Mechanotransduction at Cell-Cell Junctions. Curr Biol *28*, R445-R457.

Chen, A.F., Liu, A.J., Krishnakumar, R., Freimer, J.W., DeVeale, B., and Blelloch, R. (2018). GRHL2-Dependent Enhancer Switching Maintains a Pluripotent Stem Cell Transcriptional Subnetwork after Exit from Naive Pluripotency. Cell Stem Cell *23(2)*, 226-238.

Chen, E.Y., Tan, C.M., Kou, Y., Duan, Q., Wang, Z., Meirelles, G.V., Clark, N.R., and Ma'ayan, A. (2013). Enrichr: interactive and collaborative HTML5 gene list enrichment analysis tool. BMC Bioinformatics *14*, 128.

Chen, H., Guo, R., Zhang, Q., Guo, H., Yang, M., Wu, Z., Gao, S., Liu, L., and Chen, L. (2015). ERK signaling is indispensable for genomic stability and self-renewal of mouse embryonic stem cells. Proc Natl Acad Sci USA *112(44)*, E5936-43.

Chen, S., Lewallen, M., and Xie, T. (2013). Adhesion in the stem cell niche: biological roles and regulation. Development *140*, 255-265.

Chen, T., Yuan, D., Wei, B., Jiang, J., Kang, J., Ling, K., Gu, Y., Li, J., Xiao, L., and Pei, G. (2010). E-cadherin-mediated cell-cell contact is criticial for induced pluripotent stem cell generation. Stem Cells *28*, 1315-1325.

Chowdhury, F., Li, Y., Poh, Y.C., Yokohama-Tamaki, T., Wang, N., and Tanaka, T.S. (2010). Soft substrates promote homogenous self-renewal of embryonic stem cells via downregulating cell-matrix tractions. PLoS One *5(12)*, e15655.

Costello, I., Pimeisl, I.M., Dräger, S., Bikoff, E.K., Robertson, E.J., and Arnold, S.J. (2011). The T-box transcription factor Eomesodermin acts upstream of Mesp1 to specify cardiac mesoderm during mouse gastrulation. Nat Cell Biol *13(9)*, 1084-1091.

Dalby, M.J., Gadegaard, N., and Oreffo, R.O.C. (2014). Harnessing nanotopography and integrin-matrix interactions to influence stem cell fate. Nat Mater *13*, 558-569.

Dang, I., Gorelik, R., Sousa-Blin, C., Derivery, E., Guérin, C., Linkner, J., Nemethova, M., Dumortier, J.G., Giger, F.A., Chipysheva, T.A., et al. (2013). Inhibitory signalling to the Arp2/3 complex steers cell migration. Nature *503(7475)*, 281-284.

Di Nardo, A., Cicchetti, G., Falet, H., Hartwig, J.H., Stossel, T.P., and Kwiatkowski, D.J. (2005). Arp2/3 complex-deficient mouse fibroblasts are viable and have normal leading-edge actin structure and function. Proc Natl Acad Sci *102(45)*, 16263-16268.

De Belly, H., Stubb, A., Yanagida, A., Labouesse, C., Jones, P.H., Paluch, E.K., and Chalut, K.J. (2021). Membrane tension gates ERK-mediated regulation of pluripotent cell fate. Cell Stem Cell *28*, 273-284.

Devreotes, P., and Horwitz, A.R. (2015). Signaling networks that regulate cell migration. Cold Spring Harb Perspect Biol *7(8)*, a005959.

Dupont, S., Morsut, L., Aragona, M., Enzo, E., Giulitti, S., Cordenonsi, M., Zanconato, F., Le Digabel, J., Forcato, M., Bicciato, S. *et al*. (2011). Roll of YAP/TAZ in mechanotransduction. Nature *474*, 179-183.

Ramalho-Santos, M., Yoon, S., Matsuzaki, Y., Mulligan, R.C., and Melton, D.A. (2002). 'Stemness': transcriptional profiling of embryonic and adult stem cells. Science *298*, 597-600.

Engler, A.J., Sen, S., Sweeny, H.L., and Discher, D.E. (2006). Matrix elasticity directs stem cell lineage specification. Cell *126*, 677-689.

Esnault, C., Stewart, A., Gualdrini, F., East, P., Horswell, S., Matthews, N., and Treisman, R. (2014). Rho-actin signaling to the MRTF coactivators dominants the immediate transcriptional response to serum in fibroblasts. Genes Dev *28(9)*, 943-958.

Evans, M.J., and Kaufman, M.H. (1981). Establishment in culture of pluripotential cells from mouse embryos. Nature *292*, 154-156.

Faunes, F., Hayward, P., Descalzo, S.M., Chatterjee, S.S., Balayo, T., Trott, J., Christoforou, A., Ferrer-Vaquer, A., Hadjantonakis, A-K., Dasgupta, R. *et al*. (2013). A membrane-associated β-catenin/Oct4 complex correlates with ground-state pluripotency in mouse embryonic stem cells. Development *140*, 1171-1183.

Ganguly, A., Tang, Y., Wang, L., Ladt, K., Loi, J., Dargent, B., Leterrier, C., and Roy, S. (2015). A dynamic formin-dependent deep F-actin network in axons. J Cell Biol *210(3)*, 401-417.

Gilbert, P.M., Havenstrite, K.L., Magnusson, K.E.G., Sacco, A., Leonardi, N.A., Kraft, P., Nguyen, N.K., Thrun, S., Lutolf, M.P., and Blau, H.M. (2010). Substrate elasticity regulates skeletal muscle stem cell self-renewal in culture. Science *329*, 1078-1081.

Gilmour, D., Rembold, M., and Leptin, M. (2017). From morphogen to morphogenesis and back. Nature *541(7637)*, 311-320.

Goley, E.D., and Welch, M.D. (2006). The Arp2/3 complex: an actin nucleator comes of age. Nat Rev Mol Cell Biol *7(10)*, 713-726.

Gournier, H., Goley, E.D., Niederstrasser, H., Trinh, T., and Welch, M.D. (2001). Reconstitution of human Arp2/3 complex reveals critical roles of individual subunits in complex structure and activity. Mol Cell *8(5)*, 1041-1052.

Halder, G., Dupont, S., and Piccolo, S. (2012). Transduction of mechanical and cytoskeletal cues by YAP and TAZ. Nat Rev Mol Cell Biol *13*, 591-600.

Hamilton, W.B., Kaji, K., and Kunath, T. (2013). ERK2 suppresses self-renewal capacity of embryonic stem cells, but is not required for multi-lineage commitment. PLoS One *8(4)*, e60907.

Han, J., Yuan, P., Yang, H., Zhang, J., Soh, B.S., Li, P., Lim, S.L., Cao, S., Tay, J., Orlov, Y.L., *et al*. (2010). Tbx3 improves the germ-line competency of induced pluripotent stem cells. Nature *463(7284)*, 1096-1100.

Happe, C.L., and Engler, A.J. (2016). Mechanical Forces Reshape Differentiation Cues That Guide Cardiomyogenesis. Circ Res *118(2)*, 296-310.

Hayashi, Y., Furue, M.K., Okamoto, T., Ohnuma, K., Myoishi, Y., Fukuhara, Y., Abe, T., Sato, J.D., Hata, R-I., and Asashima, M. (2007). Integrins regulate mouse embryonic stem cell self-renewal. Stem Cells *25*, 3005-3015.

Hirano, H., and Matsuura, Y. (2011). Sensing actin dynamics: structural basis for G-actin-sensitive nuclear import of MAL. Biochem Biophys Res Commun *414(2)*, 373-378.

Huang, J., and Kalderon, D. (2014). Coupling of Hedgehog and Hippo pathways promotes stem cell maintenance by stimulating proliferation. J Cell Biol *205*, 325-338.

Hunter, J.D. (2007). Matplotlib: A 2D graphics environment. Comput Sci Eng *9(3)*, 90-95.

Hurst, V., Shimada, K., and Gasser, S.M. (2019). Nuclear Actin and Actin-Binding Proteins in DNA Repair. Trends Cell Biol *29(6)*, 462-476.

Iskratsch, T., Wolfenson, H., and Sheetz, M.P. (2014). Appreciating force and shape – the rise of mechanotransduction in cell biology. Nat Rev Mol Cell Biol *15*, 825-833.

Issigonis, M., Tulina, N., de Cuevas, M., Brawley, C., Sandler, L., and Matunis, E. (2009). JAK-STAT signal inhibition regulates competition in the *Drosophila* testis stem cell niche. Science *326*, 153-156.

Janmey, P.A., Wells, R.G., Assoian, R.K., and McCulloch, C.A. (2013). From tissue mechanics to transcription factors. Differentiation *86(3)*, 112-120.

Jurmeister, S., Baumann, M., Balwierz, A., Keklikoglou, I., Ward, A., Uhlmann, S., Zhang, J.D., Wiemann, S., and Sahin, O. (2012). MicroRNA-200c represses migration and invasion of breast cancer cells by targeting actin-regulatory proteins FHOD1 and PPM1F. Mol Cel Biol *32*, 633-651.

Kalkan, T., and Smith, A. (2014). Mapping the route from naive pluripotency to lineage specification. Philos Trans R Soc Lond B Biol Sci *369,* 20130540.

Kalkan, T., Olova, N., Roode, M., Mulas, C., Lee, H.J., Nett, I., Marks, H., Walker, R., Stunnenberg, H.G., Lilley, K.S., et al. (2017). Tracking the embryonic stem cell transition from ground state pluripotency. Development *144*, 1221-1234.

Kalkan, T., Bornelöv, S., Mulas, C., Diamanti, E., Lohoff, T., Ralser, M., Middelkamp, S., Lombard, P., Nichols, J., and Smith, A. (2019). Complementary Activity of ETV5, RBPJ, and TCF3 Drives Formative Transition from Naïve Pluripotency. Cell Stem Cell *24(5)*, 785-801.

Kan, N.G., Stemmler, M.P., Junghans, D., Kanzler, B., de Vries, W.N., Dominis, M., and Kemler, R. (2007). Gene replacement reveals a specific role for E-cadherin in the formation of a functional trophectoderm. Development *134*, 31-41.

Kartikasari, A.E.R., Zhou, J.X., Kanji, M.S., Chan, D.N., Sinha, A., Grapin-Botton, A., Magnuson, M.A., Lowry, W.E., and Bhusan, A. (2013). EMBO J *32(10)*, 1393-1408.

Kerosuo, L., Piltti, K., Fox, H., Angers-Loustau, A., Häyry, V., Eilers, M., Sariola, H., and Wartiovaara, K. (2008). Myc increases self-renewal in neural progenitor cells through Miz-1. J Cell Sci *121(23)*, 3941-3950.

Kinoshita, M., and Smith, A. (2018). Pluripotency Deconstructed. Dev Growth Differ *60(1)*, 44-52.

Kinoshita, M., Barber, M., Mansfield, W., Cui, Y., Spindlow, D., Stirparo, G.G., Dietmann, S., Nichols, J., and Smith, A. (2021). Capture of mouse and human stem cells with features of formative pluripotency. Cell Stem Cell *28(3)*, 453-471.

Keller, R., Davidson, L.A., and Shook, D.R. (2003). How we are shaped: The biomechanics of gastrulation. Differentiation *71*, 171-205.

Knoepfler, P.S., Cheng, P.F., and Eisenman, R.N. (2002). N-myc is essential during neurogenesis for the rapid expansion of progenitor cell populations and the inhibition of neuronal differentiation. Genes Dev *16(20)*, 2699-2712.

Kretzschmar, K., and Clevers, H. (2017). Wnt/β-catenin signaling in adult mammalian epithelial stem cells. Dev Biol *428*, 273-282.

Krieg, M., Arboleda-Estudillo, Y., Puech, P.H., Käfer, J., Graner, F., Müller, D.J., and Heisenberg, C.P. (2008). Tensile forces govern germ-later organization in zebrafish. Nat Cell Biol *10(4)*, 429-436.

Kuleshov, M.V., Jones, M.R., Rouillard, A.D., Fernandez, N.F., Duan, Q., Wang, Z., Koplev, S., Jenkins, S.L., Jagodnik, K.M., Lachmann, A., et al. (2016). Enrichr: a comprehensive gene set enrichment analysis web server 2016 update. Nucleic Acids Res *44(W1)*, W90-W97.

Larue, L., Ohsugi, M., Hirchenhain, J., and Kemler, R. (1994). E-cadherin null mutant embryos fail to form trophectoderm epithelium. Proc Natl Acad Sci USA *91*, 8263-8267.

Le, H.Q., Ghatak, S., Yeung, C.Y., Tellkamp, F., Günschmann, C., Dieterich, C., Yeroslaviz, A., Habermann, B., Pombo, A., Niessen, C.M., and Wickström, S.A. (2016). Nat Cell Biol *18(8)*, 864-875.

LeClair, L.L., Baumgartner, M., Iwasa, J.H., Mullins, R.D., and Barber, D.L. (2008). Phosphorylation of the Arp2/3 complex is necessary to nucleate actin filaments. J Cell Biol *182(4)*, 647-654.

LeClaire, L.L., Rana, M., Baumgartner, M., and Barber, D.L. (2015). The Nck-interacting kinase NIK increases Arp2/3 complex activity by phosphorylating the Arp2 subunit. J Cell Biol *208(2)*, 161-170.

Lee, J., Abdeen, A.A., Zhang, D., and Kilian, K.A. (2013). Directing stem cell fatr on hydrogel substrates by controlling cell geometry, matrix mechanics and adhesion ligand composition. Biomaterials *34(33)*, 8140-8148.

Li, Y., Zhu, X., Zeng, Y., Wang, J., Zhang, X., Ding, Y.Q., and Liang, L. (2010). FMNL2 enhances invasion of colorectal carcinoma by inducing epithelial-mesenchymal transition. Mol Cancer Res *8*, 1579-1590.

Liang, J., Balachandra, S., Ngo, S., and O'Brien, L.E. (2017). Feedback regulation of steady-state epithelial turnover and organ size. Nature *548*, 588-591.

Lorda-Diez, C.I., Montero, J.A., Sanchez-Fernandez, C., Garcia-Porrero, J.A., Chimal-Monroy, J., and Hurle, J.M. (2018). Four and a half domain 2 (FHL2) scaffolding protein is a marker of connective tissues of developing digits and regulates fibrogenic differentiation of lim mesodermal progenitors. J Tissue Eng Regen Med *12(4)*, e2062-e2072.

Lu, R., Yang, A., and Jin, Y. (2011). Dual functions of T-box 3 (Tbx3) in the control of self-renewal and extraembryonic endoderm differentiation in mouse embryonic stem cells. J Biol Chem *286(10)*, 8425-8436.

Lyashenko, M., Winter, M., Migliotini, D., Biechele, T., Moon, R.T., and Hartmann, C. (2011). Differential requirement for the fual functions of β-catenin in embryonic stem cell self-renewal and germ layer formation. Nat Cel Biol *13*, 753-761.

Machesky, L.M., Reeves, E., Wientjes, F., Mattheyse, F.J., Grogan, A., Totty, N.F., Burlingame, A.L., Hsuan, J.J., and Segal, A.W. (1997). Mammalian actin-related protein 2/3 complex localizes to regions of lamellipodial protrusion and is composed of evolutionarily conserved proteins. Biochem J *328*, 105-112.

Mahendram, S., Kelly, K.F., Paez-Parent, S., Mahmood, S., Polena, E., Cooney, A.J., and Doble, B.W. (2013). Ectopic γ-catenin expression partially mimics the effects of stabilized β-catenin on embryonic stem cell differentiation. PLoS One *8,* e65320.

Maritzen, T., Zech, T., Schmidt, M.S., Krause, E., Machesky, L.M., and Haucke, V. (2012). Gadkin negatively regulates cell spreading and motility via sequestration of the actin-nucleating Arp2/3 complex. Proc Natl Acad Sci USA *109(26)*, 10382-10387.

Martin, G.R. (1981). Isolation of a pluripotent cell line from early mouse embryos cultured in medium conditioned by teratocarcinoma stem cells. Proc. Natl. Acad. Sci. *78(12)*, 7634-7638.

May, R. (2001). The Arp2/3 complex: a central regulator of the actin cytoskeleton. Cell Mol Life Sci *58(11)*, 1607-1626.

McBeath, R., Pirone, D.M., Nelson, C.M., Bhadriraju, K., and Chen, C.S. (2004). Cell shape, cytoskeletal tension, and RhoA regulate stem cell lineage commitment. Dev Cell *6*, 483-495.

McDonald, M.E., Li, C., Bian, H., Smith, B.D., Layne, M.D., and Farmer, S.R. (2015). Myocardin-related transcription factor A regulates conversion of progenitors to beige adipocytes. Cell *160*, 105-118.

McGee, K.M., Vartiainen, M.K., Khaw, P.T., Treisman, R., and Bailly, M. (2011). Nuclear transport of the serum response factor coactivator MRTF-A is downregulated at tensional homeostasis. EMBO Rep *12(9)*, 963-970.

McKinney, W. (2010). Data structures for statistical computing in python. In S. van der Walt & J. Millman (Eds.), Proceedings of the 9th Python in Science Conference, 51-56.

Miralles, F., Posern, G., Zaramytidou, A.I., and Treisman, R. (2003). Actin dynamics control SRF activity by regulation of its coactivator MAL. Cell *113(3)*, 329-342.

Mohamet, L., Hawkins, K., and Ward, C.M. (2011). Loss of function of e-cadherin in embryonic stem cells and the relevance to models of tumorigenesis. J Oncol *2011*, 352616.

Molé, M.A., Weberling, A., Fässler, R., Campbell, A., Fishel, S., and Zernicka-Goetz, M. (2021). Integrin ß1 coordinates survival and morphogenesis of the embryonic lineage upon implantation and pluripotency transition. Cell Rep *34*, 108834.

Morgani, S., Nichols, J., and Hadjantonakis, A-K. (2017). The many faces of pluripotency: in vitro adaptations of a continuum of in vivo states. BMC Dev Biol *17(1)*, 7.

Morin-Kensicki, E.M., Boone, B.N., Howell, M., Stonebraker, J.R., Teed, J., Alb, J.G., Magnuson, T.R., O'Neal, W., and Milgram, S.L. (2006). Defects in yolk sac vasculogensis, chorioallantoic fusion, and embryonic axis elongation in mice with targeted disruption of Yap65. Mol Cell Biol *26*, 77-87.

Mulas, C., Kalkan, T., and Smith, A. (2017). NODAL Secures Pluripotency upon Embryonic Stem Cell Progression from the Ground State. Stem Cell Rep *9(1)*, 77-91.

Murrell, M., Oakes, P.W., Lenz, M., and Gardel, M.L. (2015). Forcing cells into shape: the mechanics of actomyosin contractility. Nat Rev Mol Cell Biol *16*, 486-498.

Myers, F.B., Silver, J.S., Zhuge, Y., Beygui, R.E., Zarins, C.K., Lee, L.P., and Abilez, O.J. (2013). Robust pluripotent stem cell expansion and cardiomyocyte differentiation via geometric patterning. Integr Biol *5*, 1495-1506.

Nakazawa, N., Sathe, A.R., Shivashankar, G.V., and Sheetz, M.P. (2016). Matrix mechanics controls FHL2 movement to the nucleus to activate p21 expression. Proc Natl Acad Sci USA *113(44)*, E6813-E6822.

Närvä, E., Stubb, A., Guzmán, C., Blomqvist, M., Balboa, D., Lerche, M., Saari, M., Otonkoski, T., and Ivaska, J. (2017). A strong contractile actin fence and large adhesions direct human pluripotent colony morphology and adhesion. Stem Cell Rep *9(1)*, 67-76.

Nichols, J., and Smith, A. (2009). Naive and primed pluripotent states. Cell Stem Cell *4(6)*, 487-492.

Nichols, J., and Smith, A. (2012). Pluripotency in the embryo and in culture. Cold Spring Harb Perspect Biol *4(8)*: a008128.

Nishimura, Y., Shi, S., Zhang, F., Liu, R., Takagi, Y., Bershadsky, A.D., Viasnoff, V., and Sellers, J.R. (2021). The formin inhibitor, SMIFH2, inhibits members of the myosin superfamily. J Cell Sci doi: 10.1242/jcs.253708, Online ahead of print.

Nishiyama, A., Sharov, A.A., Piao, Y., Amano, M., Amano, T., Hoang, H.G., Binder, B.Y., Tapnio, R., Bassey, U., Malinou, J.N., *et al*. (2013). Systematic repression of transcription factors reveals limited patterns of gene expression changes in ES cells. Sci Rep *3(1390)*, srep01390.

Niwa, H., Ogawa, K., Shimosato, D., and Adachi, K. (2009). A parallel circuit of LIF signalling pathways maintains pluripotency of mouse ES cells. Nature *460(7251)*, 118-122.

Nobusue, H., Onishi, N., Shimizu, T., Sugihara, E., Oki, Y., Sumikawa, Y., Chiyoda, T., Akashi, K., Saya, H., and Hano, K. (2014). Reglation of MKL1 via actin cytoskeleton dynamics drives adipocyte differentiation. Nat Commun *5*, 3368.

Nolen, B.J., Tomasevic, N., Russell, A., Pierce, D.W., Jia, Z., McCormick, C.D., Hartman, J., Sakowicz, R., and Pollard, T.D. (2009). Nature *460(7258)*, 1031-1034.

Ohinata, Y., Payer, B., O'Carroll, D., Ancelin, K., Ono, Y., Sano, M., Barton, S.C., Obukhanych, T., Nussenzweig, M., Tarakhovsky, A., *et al*. (2005). Blimp1 is a critical determinant of germ cell lineage in mice. Natura *436(7048)*, 207-213.

Olson, E.M., and Nordheim, A. (2010). Linking actin dynamics and gene transcription to drive cellular motile functions. Nat Rev Mol Cell Biol *11(5)*, 353-365.

O'Reilly, A.M., Lee, H-H., and Simon, M.A. (2008). Integrins control the positioning and proliferation of follicle stem cells in the *Drosophila* ovary. J Cell Biol *182*, 801-815.

Papalazarou, V., and Machesky, L.M. (2021). The cell pushes back: The Arp2/3 complex is a key orchestrator of cellular responses to environmental forces. Curr Opin Cell Biol *68*, 37-44.

Parchem, R.J., Ye, J., Judson, R.L., LaRussa, M.F., Krishnakumar, R., Blelloch, A., Oldham, M.C., and Blelloch, R. (2014). Two miRNA clusters reveal alternative paths in late-stage programming. Cell Stem Cell *14(5)*, 617-631.

Parmacek, M.S. (2007). Myocardin-related transcription factors: critical coactivators regulating cardiovascular development and adaptation. Circ Res *100*, 633-644.

Philippar, U., Schratt, G., Dieterich, C., Müller, J.M., Galgóczy, P., Engel, F.B., Keating, M.T., Gertler, F., Schüle, R., Vingron, M., and Nordheim, A. (2004). The SRF target gene Fhl2 antagonizes RhoA/MAL-depednet activation of SRF. Mol Cell *16(6)*, 867-880.

Pieters, T. and van Roy, F. (2014). Role of cell-cell adhesion complexes in embryonic stem cell biology. J Cell Sci *127(12)*, 2603-2613.

Pimental, H., Bray, N.L., Puente, S., Melsted, P., and Pachter, L. (20). Differential analysis of RNA-seq incorporating quantification uncertainty. Nat Methods *14(7)*, 687-690.

Posern, G., and Treisman, R. (2006). Actin' together: serum response factor, its cofactors and the link to signal transduction. Trends Cell Biol *16(11)*, 588-596.

Prajapati, R.S., Hintze, M., and Streit, A. (2019). PRDM1 controls the sequential activation of neural, neural crest and sensory progenitor determinants. Development *146(24)*, dev181107.

Ran, F.A., Hsu, P.D., Wright, J., Agarwala, V., Scott, D.A., and Zhang, F. (2013). Genome engineering using the CRISPR-Cas9 system. Nat Protoc *8(11)*, 2281-2308.

Rana, M.K., Aloisio, F.M., Choi, C., and Barber, D.L. (2018). Formin-dependent TGF-β signaling for epithelial to mesenchymal transition. Mol Biol Cell *29(12)*, 1465-1475.

Rauhala, H.E., Teppo, S., Niemelä, S., and Kallioniemi, A. (2013). Silencing of the ARP2/3 complex disturbs pancreatic cancer cell migration. Anticancer Res *33(10)*, 45-52.

Raymond, K., Deugnier, M-A., Faraldo, M.M., and Glukhova, M.A. (2009). Adhesion within the stem cell niches. Curr Opin Cell Biol *21*, 623-629.

Renger, A., Zafiriou, M., Noack, C., Pavlova, E., Becker, A., Sharkova, K., Bergmann, M.W., El-Armouche, A., Zimmerman, E., and Zelarayán, L.C. (2013). The Four and a Half LIM-domain 2 controls early crdiac cell commitment and expansion via regulating ß-catenin-dependent transcription. Stem Cells *31(5)*, 928-940.

Rizvi, S.A., Neidt, E.M., Cui, J., Feiger, Z., Skau, C.T., Gardel, M.L., Kozmin, S.A., and Kovar, D.R. (2009). Identification and characterization of a small molecule inhibitor of formin-mediated actin assembly. Chem Biol *16(11)*, 1158-1168.

Robinson, R.C., Turbedsky, K., Kaiser, D.A., Marchand, J.B., Higgs, H.N., Choe, S., and Pollard, T.D. (2001). Crystal structure of Arp2/3 complex. Science *294(5547)*, 1679-1684.

Rotty, J.D., Wu, C., and Bear, J.E. (2013) New insights into the regulation and cellular functions of the ARP2/3 complex. Nat Rev Mol Cell Biol *14(1)*, 7-12.

Russell, R., Ilg, M., Lin, Q., Wu, G., Lechel, A., Bergmann, W., Eiseler, T., Linta, L., Kumar, P., Klingenstein, M., *et al*. (2015). A dynamic role of Tbx3 in the pluripotency circuitry. Stem Cell Rep *5(6)*, 1155-1170.

Sanjana, N.E., Shalem, O., and Zhang, F. (2014). Improved vectors and genome-wide libraries for CRISPR screening. Nat Methods *11(8)*, 783-784.

Schratt, G., Phillippar, U., Berger, J., Schwarz, H., Heidenreich, O., and Nordheim, A. (2002). Serum response factor is crucuail for actin cytoskeletal organization and focal adhesion assembly in embryonic stem cells. J Cell Biol *156(4)*, 737-750.

Sen, B., Xie, Z., Uzer, G., Thompson, W.R., Styner, M., Wu, X., and Rubin, J. (2015). Intranuclear Actin Regulates Osteogenesis. Stem Cells *33(10)*, 3065-3076.

Shaw, R.L., Kohlmaier, A., Polesello, C., Veelken, C., Edgar, B.A., and Tapon, N. (2010). The Hippo pathway regulates intestinal stem cell proliferation during *Drosophila* adult midgut regeneration. Development *137*, 4147-4158.

Smith, A. (2017). Formative pluripotency: the executive phase in a developmental continuum. Development *144*, 365-373.

Sokolova, O.S., Chemeris, A., Guo, S., Alioto, S.L., Gandhi, M., Padrick, S., Pechnikova, E., David, V., Gautreau, A., and Goode, B.L. (2017). Structural basis

of Arp2/3 complex inhibition by GMF, coronin, and arpin. J Mol Biol *429(2)*, 237-248.

Soncin, F., Mohamet, L., Ritson, S., Hawkins, K., Bobola, N., Zeef, L., Merry, C.L.R., and Ward, C.M. (2011). E-cadherin acts as a regulator of transcripts associated with a wide range of cellular processes in mouse embryonic stem cells. PLoS One *6*, e21463.

Soncin, F., and Ward, C.M. (2011). The function of e-cadherin in stem cell pluripotenct and self-renewal. Genes *2*, 229-259.

Song, X., Zhu, C-H., Doan, C., and Xie, T. (2002). Germline stem cells anchored by adherens junctions in the *Drosophila* ovary niches. Science *296*, 1855-1857.

Song, X., and Xie, T. (2002). DE-cadherin-mediated cell adhesion is essential for maintaining somatic stem cells in the *Drosophila* ovary. Proc Natl Acad Sci USA *99*, 14813-14818.

Spencer, H.L., Eastham, A.M., Merry, C.L.R., Southgate, T.D., Perez-Campo, F., Soncin, F., Ritson, S., Kemler, R., Stern, P.L., and Ward, C.M. (2007). E-cadherin inhibits cell surface localization of the pro-migratory 5T4 oncofetal antigen in mouse embryonic stem cells. Mol Biol Cell *18*, 2838-2851.

Staley, B.K., and Irvine, K.D. (2010). Warts and Yorkie mediate intestinal regeneration by influencing stem cell proliferation. Curr Biol *20*, 1580-1587.

Steffen, A., Faix, J., Resch, G.P., Linkner, J., Wehland, J., Small, J.V., Rottner, K., and Stradal, T.E. (2006) Filopodia formation in the absence of functional WAVE- and Arp2/3-complexes. Mol Biol Cell *17(6)*, 2581-2591.

Stephenson, R.O., Yamanaka, Y., and Rossant, J. (2010). Disorganized polarity and excess trophectoderm cell fate in preimplantation embryos lacking E-cadherin. Development *137*, 3383-3391.

Sun, Q., Chen, G., Streb, J.W., Long, X., Yang, Y., Stoeckart, C.J. Jr., and Milano, J.M. (2006). Defining the mammalian CArGome. Genome Res *16(2)*, 197-207.

Sun, X., Phua, D.Y.Z., Axiotakis, Jr., L., Smith, M.A., Blankman, E., Gong, R., Cail, R.C., Espinosa de los Reyes, S., Beckerle, M.C., Waterman, C.M., and Alushin, G.M. (2020). Mechanosensing through direct binding of tensed F-actin by LIM domains. Dev Cell *55*, 1-15.

Suraneni, P., Rubinstein, B., Unruh, J.R., Durnin, M., Hanein, D., and Li, R. (2012). The Arp2/3 complex is required for lamellipodia extension and directional fibroblast cell migration. J Cell Biol *197(2)*, 239-251.

Swaney, K.F., and Li, R. (2016). Function and regulation of the Arp2/3 complex during cell migration in diverse environments. Curr Opin Cell Biol *42*, 63-72.

Tanentzapf, G., Devenport, D., Godt, D., and Brown, N.H. (2007). Integrin-dependent anchoring of a stem-cell niche. Nat Cell Biol *9*, 1413-1418.

Tatapudy, S., Aloisio, F., Barber, D., and Nystul, T. (2017). Cell fate decisions: emerging roles for metabolic signals and cell morphology. EMBO Rep *18(20)*, 2105-2118.

Tosic, J., Kim, G., Pavlovic, M., Schröder, C.M., Mersiowsky, S, Barg, M., Hofherr, A., Probst, S., Köttgen, M., Hein, L., and Arnold, S.J. (2019). Eomes and Brachyury control pluripotency exit and germ-layer segregation by changing the chromatin state. Nat Cell Biol *21*, 1518-1531.

Uda, Y., Poh, Y-C., Chowdhury, F., Wu, D.C., Tanaka, T.S., Sato, M., and Wang, N. (2011). Force via integrins but not E-cadherin decreases Oct3/4 expression in embryonic stem cells. Biochem Biophys Res Commun *415*, 396-400.

Vartiainen, M.K., Guettler, S., Larijani, B., and Treisman, R. (2007). Nuclear actin regulates dynamic subcellular localization and activity of the SRF cofactor MAL. Science *316(5832)*, 1749-1752.

Verma, S., Han, S.P., Michael, M., Gomez, G.A., Yang, Z., Teasdale, R.D., Ratheesh, A., Kovacs, E.M., Ali, R.G., and Yap, A.S. (2012). A WAVE2-Arp2/3 actin nucleator apparatus supports junctional tension at the epithelial zonula adherens. Mol Biol Cel *23(23)*, 4601-4610.

Villegas, F., Lehalle, D., Mayer, D., Rittirsch, M., Stadler, M.B., Zinner, M., Olivieri, D., Vabres, P., Duplomb-Jego, L., De Bont, E.S.J.M., et al. (2019). Lysosomal Signaling Licenses Embryonic Stem Cell Differentiation via Inactivation of Tfe3. Cell Stem Cell *24(2)*, 257-270.

Villeneuve, C., Wickström, S.A. (2021). Shaping the stem cell field. Nat Rev Mol Cell Biol *22,* 305.

Voog, J., D'Alterio, C., and Jones, D.L. (2008). Multipotent somatic stem cells contribute to the stem cell niche in the *Drosophila* testis. Nature *454*, 1132-1136.

Wagh, K., Ishikawa, M., Garcia, D.A., Stavreva, D.A., Upadhyaya, A., and Hager, G.L. (2021). Mechanical regulation of transcription: Recent Advances. Trends Cell Biol *31(6)*, 457-472.

Wang, D.Z., Li, S., Hockemeyer, D., Sutherland, L., Wang, Z., Schratt, G., Richardson, J.A., Nordheim, A., and Olson, E.N. (2002). Potentiation of serum response

factor activity by a family of myocardin-related transcription factors. Proc Natl Acad Sci USA *99(23)*, 14855-14860.

Waskom, M.L. (2021). Seaborn: statistical data visualization. J Open Source Softw *6(60)*, 3021.

Weidgang, C.E., Russell, R., Tata, P.R., Kühl, S.J., Illing, A., Müller, M., Lin, Q., Brunner, C., Boeckers, T.M., Bauer, K., *et al*. (2013). TBX3 directs cell-fate decision toward mesendoderm. Stem Cell Rep *1(3)*, 248-265.

Weinberger, L., Ayyash, M., Novershtern, N., and Hanna, J.H. (2016). Dynamic stem cell states: naive to primed pluripotency in rodents and humans. Nat Rev Mol Cell Biol *17(3)*, 155-169.

Weinhold, B., Schratt, G., Arsenian, S., Berger, J., Kamino, K., Schwarz, H., Rüther, U., and Nordeim, A. (2000). Srf-/- ES cells display non-cell-autonomous impairment in mesodermal differentiation. EMBO J *19(21)*, 5835-5844.

Welch, M.D., De Pace, A.H., Verma, S., Iwamatsu, A., and Mitchison, T.J. (1997). The human Arp2/3 complex is composed of evolutionarily conserved subunits and is localized to cellular regions of dynamic actin filament assembly. J Cell Biol *138*, 375-384.

Welch, M.D., and Mullins, R.D. (2002). Cellular control of actin nucleation. Annu Rev Cell Dev Biol *18*, 247-288.

Wray, J., Kalkan, T., Gomez-Lopez, S., Eckardt, D., Cook, A., Kemler, R., and Smith, A. (2011). Inhibition of glycogen synthase kinase-3 alleviates Tcf3 repression of the pluripotency network and incrrases embryonic stem cell resistance to differentiation. Nat Cell Biol *13*, 838-845.

Xi, R. (2009). Anchoring stem cells in the niche by cell adhesion molecules. Cell Adh Migr *3*, 396-401.

Xia, S., Lim, Y.B., Zhang, Z., Wang, Y., Zhang, S., Lim, C.T., Yim, E.K.F., Kanchanawong, P. (2019). Nanoscale architecture of the cortical actin cytoskeleton in embryonic stem cells. Cell Rep *28*, 1251-1267.

Yang, Q., Zhang, X.F., Pollard, T.D., and Forscher, P. (2012). Arp2/3 complex-dependent actin networks constrain myosin II function in driving retrograde actin flow. J Cell Biol *197(7)*, 939-956.

Ying, Q.L., Wray, J., Nichols, J., Batlle-Morera, L., Doble, B., Woodgett, J., Cohen, P., and Smith, A. (2008). The ground state of embryonic stem cell self-renewal. Nature *453(7194)*, 519-523.

Ying, Q-L., and Smith, A. (2017). The art of capturing pluripotency: creating the right culture. Stem Cell Reports *8*, 1457-1464.

Yoo, Y., Wu, X., and Guan, J.L. (2007). A novel role of the actin nucleating Arp2/3 complex in the regulation of RNA polymerase II-dependent transcription. J Biol Chem *282(10)*, 7616-7623.

Zoldan, J., Karagiannis, E.D., Lee, C.Y., Anderson, D.G., Langer, R., and Levenberg, S. (2011). The influence of scaffold elasticity on germ layer specification of human embryonic stem cells. Biomaterials *32*, 9612-9621.

Publishing Agreement

It is the policy of the University to encourage open access and broad distribution of all theses, dissertations, and manuscripts. The Graduate Division will facilitate the distribution of UCSF theses, dissertations, and manuscripts to the UCSF Library for open access and distribution. UCSF will make such theses, dissertations, and manuscripts accessible to the public and will take reasonable steps to preserve these works in perpetuity.

I hereby grant the non-exclusive, perpetual right to The Regents of the University of California to reproduce, publicly display, distribute, preserve, and publish copies of my thesis, dissertation, or manuscript in any form or media, now existing or later derived, including access online for teaching, research, and public service purposes.

Francesco Mori Aloisio
Author Signature

6/8/2021
Date